Ph.D. Thesis

Growth, Processing and In-situ Observation of Graphene

（グラフェンの成長、加工とその場観察に関する研究）

Mikihiro Kato

Department of Physics, Graduate School of Science

Tokyo University of Science

1-3 Kagurazaka, Shinjuku-ku, Tokyo 162-8601, Japan

Contents

Abstract

Graphene has many unique properties, such as high electric mobility, transparency and high thermolability. It has been attracting attention for using in the next generation electronic devices material. For industrial utilization of graphene, researches by theory and by experiment are still necessary. In addition, for obtaining easy and efficient fabrication method of graphene, observation (evaluation) and processing technique are important. In this work, the experiments were conducted focusing on growth, processing and in-situ observation of graphene.

About growth, we proposed a method to synthesize graphite thin layer by using deposited organic solution which includes benzene rings. Single and multi layer graphene sample were successfully fabricated by this organic coating method. For observation, we developed a method of in-situ observation by using an optical microscope (OM). This OM observation enabled us to study the growth mechanism including. We also studied the stability of graphenen layers at high temperature heating. Our results provide a new way to study the growth and change of graphene material. In the third part of the paper, we showed the anodic oxidation of graphene layers. Due to the different layer numbers of graphene, different oxidation behaviors were observed. A model was proposed to explain this different phenomenon.

Although this paper in focused on the growth, processing and in-situ observation, there are still many unknown propertied of this matrial. Even for that, our study must be a pioneer approach to observe the growth dynamics of graphene in an easy way.

Preface

Study of graphite has a long history of hundred years, and it has been widely used as polarized materials that transmit electricity. Graphene was recognized as the basic constituent of graphite from a long time ago, and a theoretical study about the electronic property was performed at 1940 decade, after the Second World War, and an electronic structure of graphene was announced in 1947.

From the 1970 to the 1980's, the studies of high conductivity and superconductivity are manifested by intercalating variety substances into a graphite layer. These results, led to a growing interest of materials technology persons.

In the 1990’s, graphene became conscious in the flow of a study about a carbon nanotube (CNT). Andre Geim of Manchester University succeeded in production of graphene by detaching a Scotch tape and made an innovative experiment in 2004. The first report of monolayer graphene was given by Nobselov et al. [1], the Nobel Prize work of 2010. Graphene has large carrier mobility (about 200,000 $cm^2V^{-1}s^{-1}$) at room temperature (RT), which is 100 times as that of Si. These findings have led research into graphene worldwide. It is now the hottest subject because of its use as an industrial material.

Chapter 1. Introduction

1.1 Crystal structure and electronic orbits of graphene

Carbon is a nonmetallic element of atomic number 6 and belongs to the 14th group element and the 2nd cycle in a periodic table. It can form a maximum of four covalent bonds with other elements to form various molecules. There are about 54,000,000 kinds of compounds related to carbon and other elements. Carbon is a surprisingly versatile element, able to hybridize in three different states, sp^1, sp^2 and sp^3. The changes in local bonding of carbon atoms account for the existence of extremely diverse allotropic phases, exhibiting a quite broad range of physical and chemical properties [2-4].

Graphene is an one-atom-thick planar sheet of sp^2-bonded carbon atoms that are densely packed in a honeycomb crystal lattice. It is the basic structural element of some carbon allotropes included in graphite, carbon nanotubes (CNT) and fullerenes. In Fig. 1 (a), (b) and (c), the unit cell and Brillouin zone of graphene are shown. $\mathbf{a_1}$ and $\mathbf{a_2}$ are unit vectors in real

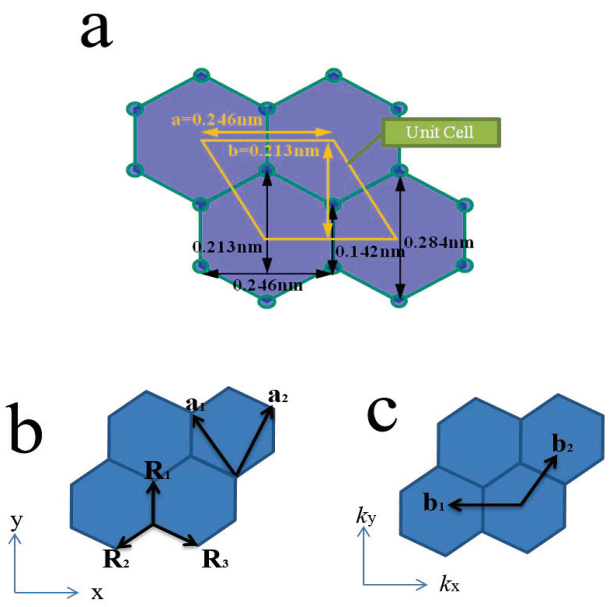

Fig. 1 The unit cell, unit vectors in real space and the Brillouin zone of graphene

space,

$$\mathbf{a_1} = \left(\frac{\sqrt{3}\mathrm{a}}{2}, \frac{\mathrm{a}}{2}\right) \ , \mathbf{a_2} = \left(\frac{\sqrt{3}\mathrm{a}}{2}, -\frac{\mathrm{a}}{2}\right)$$

where $\mathbf{b_1}$ and $\mathbf{b_2}$ are reciprocal lattice vectors. The distance between two neighboring carbon atoms is 0.142 nm.

$$\boldsymbol{b_1} = \left(\frac{2\pi}{\sqrt{3}\mathrm{a}}, \frac{2\pi}{\mathrm{a}}\right), \boldsymbol{b_2} = \left(\frac{2\pi}{\sqrt{3}\mathrm{a}}, -\frac{2\pi}{\mathrm{a}}\right)$$

The Hamiltonian for the crystal is given by the following equation:

$$H = -\frac{h^2}{2m}\nabla^2 + v(r) \qquad (1.1.1)$$

The first term describes the kinetic energy of electrons, and the second term represents the periodic potential in the crystal. In the following equation, the electronic state in the periodic potential is handled by a tight binding method. There are two different atoms in the unit cell of graphite:

$$|\psi_k\rangle = C_k^A|\psi_k^A\rangle + C_k^B|\psi_k^B\rangle \qquad (1.1.2)$$

where $\psi_k^\alpha\rangle \ \alpha = A, B$ are Bloch functions in their respective sublattices. The following is represented by the tight binding method:

$$\psi_k^\alpha\rangle = \frac{1}{\sqrt{N_u}} \sum_{\boldsymbol{r}_i \in \alpha} e^{i\boldsymbol{k}\cdot\boldsymbol{r}_i} \emptyset(\boldsymbol{r} - \boldsymbol{r_i}) \qquad (\alpha = A, B) \qquad (1.1.3)$$

Here $\emptyset(\boldsymbol{r} - \boldsymbol{r_i})$ is the wave function of the π electron in the atom localized at the position $\boldsymbol{r_i}$ and N_u is the unit lattice in the crystal. From this, the eigenenergy E_k corresponding to the quantum number k can be

obtained. According to the variational principle in quantum mechanics, the energy eigenvalues are obtained as follows:

$$E_k = \frac{\langle\psi_k|H|\psi_k\rangle}{\langle\psi_k|\psi_k\rangle} = \frac{\sum_{\alpha,\beta} C_k^{\beta*} C_k^{\alpha} \left\langle\psi_k^{\beta}\middle|H\middle|\psi_k^{\alpha}\right\rangle}{\sum_{\alpha,\beta} C_k^{\beta*} C_k^{\alpha} \left\langle\psi_k^{\beta}\middle|\psi_k^{\alpha}\right\rangle} \qquad (1.1.4)$$

The necessary condition for obtaining the minimum value is that the differential coefficient becomes zero.

$$\frac{\partial E_k}{\partial C_k^{\beta*}}$$

$$= \frac{\left[\sum_{\alpha} C_K^{\alpha} \left\langle\psi_K^{\beta}\middle|H\middle|\psi_K^{\alpha}\right\rangle \sum_{\alpha',\beta'} C_K^{\beta'*} C_K^{\alpha'} \left\langle\psi_K^{\beta'}\middle|\psi_K^{\alpha'}\right\rangle - \sum_{\alpha,\beta'} C_K^{\beta'*} C_K^{\alpha} \left\langle\psi_K^{\beta'}\middle|H\middle|\psi_K^{\alpha}\right\rangle \sum_{\alpha'} C_K^{\alpha'} \left\langle\psi_K^{\beta}\middle|\psi_K^{\alpha'}\right\rangle\right]}{\left[\sum_{\alpha,\beta} C_K^{\beta*} C_K^{\alpha} \left\langle\psi_K^{\beta}\middle|\psi_K^{\alpha}\right\rangle\right]^2}$$

$$= \sum_{\alpha,\alpha',\beta'} \frac{C_K^{\alpha'} C_K^{\beta'*} \left\langle\psi_K^{\beta'}\middle|\psi_K^{\alpha'}\right\rangle \left[\left\langle\psi_K^{\beta}\middle|H\middle|\psi_K^{\alpha}\right\rangle - E_K \left\langle\psi_K^{\beta}\middle|\psi_K^{\alpha}\right\rangle\right] C_K^{\alpha}}{\left[\sum_{\alpha,\beta} C_K^{\beta*} C_K^{\alpha} \left\langle\psi_K^{\beta}\middle|\psi_K^{\alpha}\right\rangle\right]^2} = 0 \qquad (1.1.5)$$

The equation gives the energy eigenvalue,

$$det[H - ES] = 0 \qquad (1.1.6)$$

The Hamiltonian matrix $H_{\alpha\beta}(\mathbf{K}) = \left\langle\psi_{\boldsymbol{K}}^{\boldsymbol{\alpha}}\middle|\boldsymbol{H}\middle|\psi_K^{\beta}\right\rangle$ and the overlap integral matrix $S_{\alpha\beta}(K) = \left\langle\psi_K^{\alpha}\middle|\psi_K^{\beta}\right\rangle$ is introduced into equation (1.1.6). Expanding the coefficients of energy eigenvalues and wavefunctions can be done by solving the equations. The Hamiltonian matrix is represented by a 2 × 2 matrix by taking $\left|\psi_K^{\mathrm{A}}\right\rangle, |\psi_K^{B}\rangle$ as a basis.

$$H = \begin{pmatrix} H_{AA} & H_{AB} \\ H_{BA} & H_{BB} \end{pmatrix} \qquad (1.1.7)$$

By ignoring the second-order or more terms of the H_{AA} component and by considering only on-site integration, it can be expressed as follows:

$$H_{AA} = \langle \psi_K^A | H | \psi_K^A \rangle$$

$$= \frac{1}{N_u} \sum_{r_A, r'_A} e^{i\boldsymbol{K}(\boldsymbol{r_A} - \boldsymbol{r'_A})} \langle \phi(r - r'_A) | H | \phi(r - r_A) \rangle$$

$$= \frac{\varepsilon_{2p}}{N_u} \sum_{r_A} 1$$

$$= \varepsilon_{2p} \qquad (1.1.8)$$

The (A,B) component is

$$H_{\mathrm{AB}} = \langle \psi_K^A | H | \psi_K^B \rangle$$

$$= \frac{1}{N_u} \sum_{r_A, r_B} e^{i\mathbf{k}(\mathrm{r}_B - r_A)} \langle \phi(r - r_A) | H | \phi(r - r_B) \rangle$$

$$= \frac{\gamma_0}{N_u} \sum_{r_A} \sum_{i=1,2,3} e^{i\mathbf{K}\mathbf{R}_i} = \gamma_0 f(\mathbf{K}) \qquad (1.1.9)$$

$\gamma_0 = \langle \phi(\boldsymbol{r}) | H | \phi(\boldsymbol{r} - \boldsymbol{R}_i) \rangle$ is the hopping integral between nearest neighbor atoms $(\gamma_0 < 0)$. The function $f(\boldsymbol{K})$ is introduce:

$$f(\boldsymbol{K}) = \sum_{i=1}^{3} e^{i\boldsymbol{k}\cdot R_i} = e^{ik_x a/\sqrt{3}} + 2e^{-ik_x a/2\sqrt{3}} \cos\frac{a}{2} \qquad (1.1.10)$$

The Schroedinger equation may be written in the matrix form:

$$\begin{pmatrix} \varepsilon_{2p} & \gamma_0 f(\boldsymbol{K}) \\ \gamma_0 f^*(\boldsymbol{K}) & \varepsilon_{2p} \end{pmatrix} \begin{pmatrix} C_K^A \\ C_K^B \end{pmatrix}$$

$$= E \begin{pmatrix} 1 & sf(\boldsymbol{K}) \\ sf^*(\boldsymbol{K}) & 1 \end{pmatrix} \begin{pmatrix} C_K^A \\ C_K^B \end{pmatrix} \qquad (1.1.11)$$

The non-trivial solution is given by solving the secular equation of equation (1.1.11), that is, equation (1.1.6). The energy eigenvalues are thus expressed as follows:

$$\begin{vmatrix} \varepsilon_{2p} - E & f(\boldsymbol{K})(\gamma_0 - sE) \\ f^*(\boldsymbol{K})(\gamma_0 - sE) & \varepsilon_{2p} - E \end{vmatrix} = 0 \qquad (1.1.12)$$

$$E_K = \frac{\varepsilon_{2p} \pm \gamma_0 \omega(\boldsymbol{K})}{1 \pm s\omega(\boldsymbol{K})} \qquad (1.1.13)$$

In equation (1.1.13), the positive sign corresponds to the energy eigenvalue of the valence band and the negative sign corresponds to the energy eigenvalue of the conduction band, respectively.

$$\omega(\boldsymbol{K}) = \sqrt{|f(\boldsymbol{K})|^2} = \sqrt{1 + 4\cos\frac{\sqrt{3}k_x a}{2}\cos\frac{k_y a}{2} + 4\cos^2\frac{k_y a}{2}} \qquad (1.1.14)$$

This formula is used in a three-dimensional plot in Fig. 2.

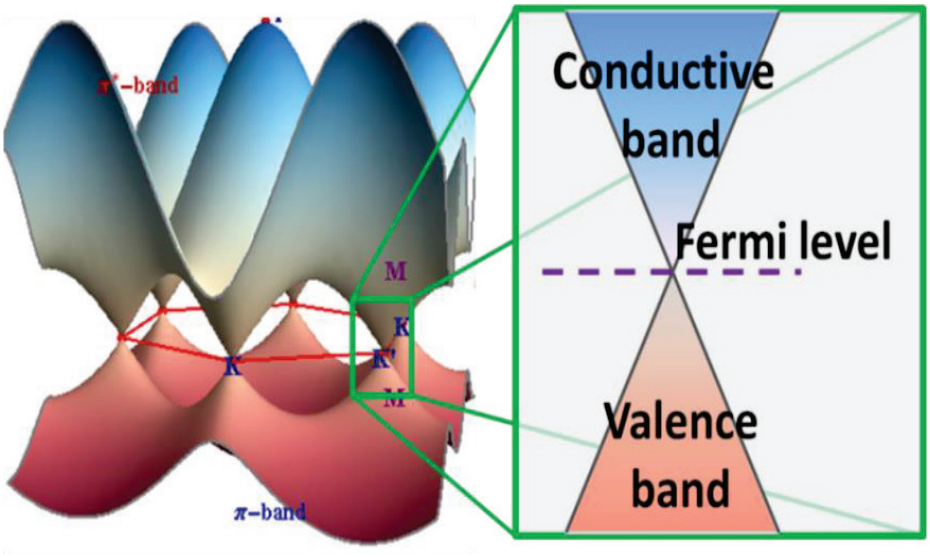

Fig. 2 Band structure of graphene

1.2 Properties of graphene

1) Electronic properties

As described in the previous part, intrinsic graphene is a semi-metal or zero-gap semiconductor, because its conduction and valence bands meet at the Dirac points. Understanding the electronic structure of graphene is the starting point for finding the band structure of graphite. It was realized early on that the E-k relation is linear for low energies near the six corners of the two-dimensional hexagonal Brillouin zone, leading to zero effective mass for electrons and holes [5-7].

2) Optical properties

Despite that graphene comprises a thin film of one atomic layer, it is visible to the naked eye. Graphite peeled by the Scotch tape method and transferred to a substrate has been observed under an optical microscope in the previous works [8,9]. Light absorption of graphene is caused by photo excitation from the valence band to the conduction band. In general, the absorptance when light of the frequency ω is vertically transmitted to a two-dimensional system is approximately given by the following equation.

$$\eta = \frac{4\pi}{c}\mathrm{Re}\sigma(\omega)$$

Here, c is the speed of light, $\sigma(\omega)$ is the electric conductivity with respect to the oscillating electric field. The electrical conductivity is a complex number, and Re means to take a real part.

The electric mobility in single-layer graphene has been reported to be a constant value independent of ω; thus, the absorbance is also a constant value as described in the equation below:

$$\eta = \frac{\pi e^2}{\hbar c} \sim 2.3\%$$

This behavior is a result of the exceptional low energy electronic structure of monolayer graphene characterized by a conical band structure at Dirac point [10,11].

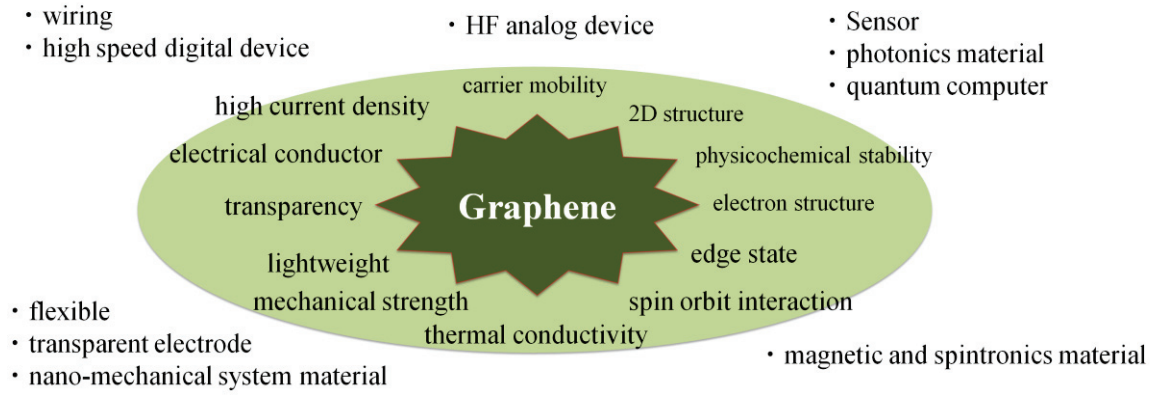

Fig. 3 Potential applications of graphene

Graphene has many other excellent properties, such as high thermal conductivity, mechanical characteristic, quantum Hall effect and etc. Thus, it has been attracting attention as a new material for next generation electronic devices. The properties of graphene are expected to make various applications, as shown in Fig. 3. For example, graphene is almost transparent even with several layers, it is flexible and passes electricity well. For that reason, applications to flexible transparent electrodes are being studied for applications such as touch screens and solar cells. High carrier mobility is suitable for high-speed electronics. However, graphene is difficult to turn off current, so application research on analog high frequency devices is progressing. It is also promising for photonics elements such as photodetectors and modulators. Besides, there are various potential applications such as sensors, wiring, heat dissipation, capacitors and membranes [12-17].

1.3 General method of graphene synthesis

Production of graphene is tried by various approaches by many study groups even at present. General making methods are introduced here below.

1) Mechanical exfoliation

Mechanical exfoliation of highly oriented pyrolytic graphite (HOPG) provides the best quality graphene. The first time of graphene reported used this method, to peel graphite with a tape many times. Although it can not be said that efficiency is good, it is attractive because it does not need an expensive equipment and get a useful sample in a very simple way. Initially it was able to produce only ones with several micrometers in size. With refinement of technique people can produce of a 100 μm size sample in nowadays [18].

2) Epitaxial growth from SiC substrate

The fabrication of graphite from SiC was reported by Acheson firstly [19]. The growth mechanism has been investigated since the 1960s [20]. Few years later, many research groups reported the production of graphene films by thermal decomposition of SiC at temperature higher than ~1350 °C in ultra-high vacuum (UHV). Graphene grown on either of the two polar faces of 4H-SiC or 6H-SiC wafer, the SiC (0001) silicon terminated surface and the SiC($000\bar{1}$) carbon terminated surface, shows that these films behave like graphene. The interesting feature of UHV Si-face grown graphene is that the number of layers grown is relatively insensitive to the time and seems to only depend on the growth temperature. On the other hand, that of the C-face graphene depends on both temperature and growth time [21]. Growth of graphene on SiC is usually referred to as epitaxial growth.

3) Chemical vapor deposition (CVD)

CVD is a widely used technique for deposition or growth of thin films, being the mainstream technique for depositing materials used in semiconductor devices for decades. There are different types of CVD processes. For example, thermal, plasma, cold-wall, hot-wall, reactive, etc. The thermal CVD method combined with the roll-to-roll process [22] enables continuous synthesis of graphene on a long copper (Cu) foil. The growth process of graphene is well known as using a nickel (Ni) or Cu catalyst. In the case of using the Ni substrate, carbon sources are first dissolved in Ni at high temperatures. After that, graphene grows on the Ni surface during the cooling process [23,24]. On the other hand, the use of Cu substrate enables a monolayer graphene formation, which is caused by the low carbon solubility in Cu at high temperatures [25,26].

In addition, there are a variety of production ways. For example, molecular beam epitaxy growth, atomic layer epitaxy, chemical synthesis etc [27-30].

Table. 1
Physical properties and application examples of graphene by each method.

Method	**Graphene size (μ m)**	**Property ($cm^2V^{-1}s^{-1}$)**	**Applications**
Mechanical exfoliation	~1000	~120,000 (@ 240 K)	Fundamental research
Growth on SiC	~100	~15,000 (@ RT)	Transistors, other electronic devices
CVD	~50000	~10,000 (@ RT)	Photonics, nanoelectronics, sensors, bio-applications

Although synthesis by CVD is the mainstream method at present, it requires a long growth time, and its technique of transfer to other substrates still presents problems [31,32]. Hence, the process of organic solution coating is reported here. This technique can be incorporated into existing

semiconductor manufacturing process. It also does not need an efficient and expensive system. This method can provide a simple, quick way of producing graphene layers with low cost.

There are other production methods on the preparation side of graphene, but there have been reports on polymers [33] and organosilane gases [34,35], but production from specific organic substances containing benzene rings was not reported before this study. If graphene can be obtained by coating an organic substance containing a benzene ring and subjecting it to heat treatment, there is a possibility that it can be directly produced on a substrate without using a metal catalyst. However, high temperature and high pressure are usually required for graphitization of organic matter. As the first step, we chose Orange II as the organic matter and coated in on Ni substrate to investigate the possibility of graphene growth at relatively lower temperature that the present methods. Most of our aims were realized and the low temperature growth of graphene such as ~ 800 ºC was demonstrated.

1.4 General processing method of graphene

There has been considerable interest in the nano-processing of graphene [36,37]. Focused ion beam (FIB) is widely used as a rapid prototyping tool for micro and nano electronic devices and for circuit repair as the technique enables site-specific removal and deposition of material. In general, Milling or sputtering is achieved through collisions of the energetic Ga^{+} ions with the target atoms, displacing them from their original sites. The higher the acceleration voltage, the narrower the beam can be. However, the damage to the sample will increase or will dope the graphene sample. To reduce the damage of the sample, another ion source such as Helium (He) is used. Although high precision processing can be achieved, it is an expensive apparatus and it is necessary to have a vacuum lower than 10^{-4} Pa at the minimum. Besides, several different graphene patterning and processing method have been developed. For example, catalytic cutting technique, plasma etching, electron beam etching and so on [38- 40]. In this work, we focused on the technique called AFM anodic oxidation. This technique will perform high-resolution patterning and processing compared will ion and electron beams.

Chapter 2. Fabrication of graphene films from organic coating

As mentioned in the previous chapter, the efficiency of graphene production is an important problem. In this section, methods of graphene synthesis using organic coatings are proposed.

2.1. About organic matter of this method

The commercialy sold Orange II was used as the starting material. It is named as Acid Orange 7 ($C_{16}H_{11}N_2NaO_4S$). Details are indicated below.
It is also named as p-(2-Hydroxy-1-naphthylazo) benzenesufonic Acid Sodium Salt. Its molecular weight is 350.32, the melting point is 164 °C and the solubility is 116 g/l (in water at 30 °C).

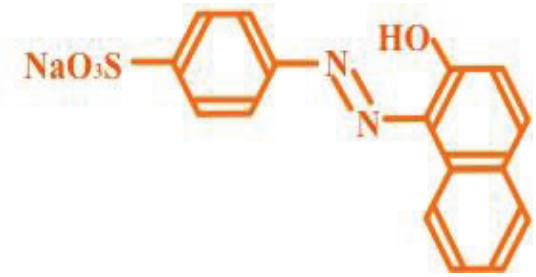

Fig. 4 Structural formula of Orange II

Its orange color is due to its azo group (-N=N-). There are three reasons for its use in the study. Firstly, coating of the substrate surface by the dye can be judged from its color. Secondly, it is readily available and inexpensive. Third, the structure of orange II tends to be planar. Organic compounds with benzene rings flanking the azo group usually have geometric isomers (i.e., *cis* and *trans* structures). However, the naphthalene ring of orange II exhibits steric hindrance (Fig. 5). Therefore, it only occurs as a *trans* isomer. From such reasons, we chose this organic matter.

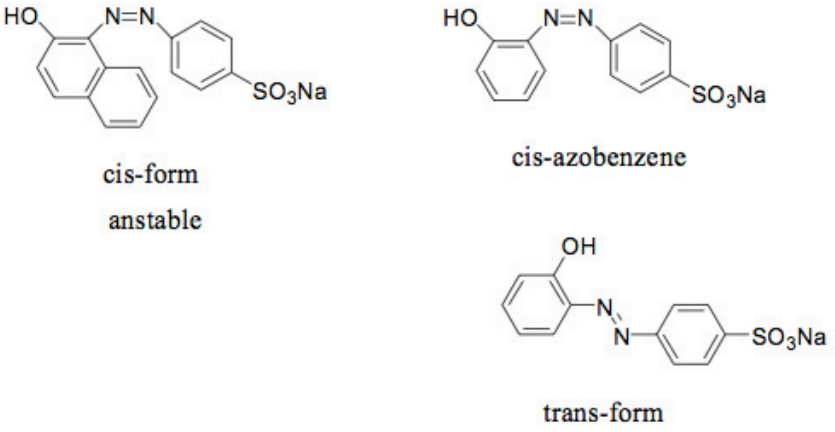

Fig. 5 steric hindrance of Orange II

2.2 Sample preparation

As first preparation, the Si (100) wafer was heated at a temperature of 1000 ºC for 10 hours in air by using a muffle furnace. A Si (100) substrate with an oxide layer of 250 – 300 nm thickness on its surface was used as the starting material. After organical cleaning of the Si (100) substrates, pure Ni was deposited on the oxide surface. Two techniques were used to deposit the Ni layers, which were named as, vacuum deposition and magnetron sputtering. The Ni layers were used as catalyst for graphene formation. Pure Ni metal having a thickness of 100 nm was deposited onto SiO_2 in vacuum at a background pressure of 10^{-4} Pa. During Ni sputtering, the substrate was kept at room temperature (RT) and/or heated up to 500 °C. The plasma power was 150 W, and the deposition time was 25 min. The flow rate of Ar gas was maintained at 10.0 ml/min, and the pressure was kept at 0.65 Pa. Afterward, the Si wafer was dipped in an acetone-saturated solution of orange II. The $Ni/SiO_2/Si$ surface was coated with orange II by simple dipping. The dipping process was as same as that used for the Ni film deposited in vacuo and the Ni film formed by sputtering. The two samples were then annealed in vacuo (about 10^{-4} Torr) at 850 °C for 5 min

under an IR lamp to thermally decompose the orange II and to form graphene. The rate of temperature increase was approximately 2.77 °C/s. Conditions such as heat treatment temperature, heating time, cooling time, difference of the film thickness of the Ni, etc. were investigated to optimize the fabrication conditions.

2.3 Evaluation methods and results

2.3.1 Raman spectroscopy

Raman spectroscopy is a spectroscopic technique used to observe vibrational, rotational, and other low-frequency modes in a system. From such results molecules can be identified. A Raman scattering (observed in Raman spectra) of carbon materials gives us various information. The most famous Raman peaks of graphene and graphite are the so-called G-band appearing at 1582 cm^{-1}, the D-band at about 1350 cm^{-1}, G'(2D)-band at about 2700 cm^{-1} [41,42]. If we see the G-band in the Raman spectra, we can say that sample contains sp^2 carbon networks. Moreover, crystallinity can be judged from existence of D-band. The number of rough layers can be judged from the peak intensity ratio of G-band and G'-band. Figure 6 shows the equipment (JASCO) used for Raman spectroscopy. Raman measurement conditions were mainly lens magnification 100×, excitation wavelength 532.30 nm, slit width 0.1 × 6 mm, exposure time 60 sec and cumulated number 2 times.

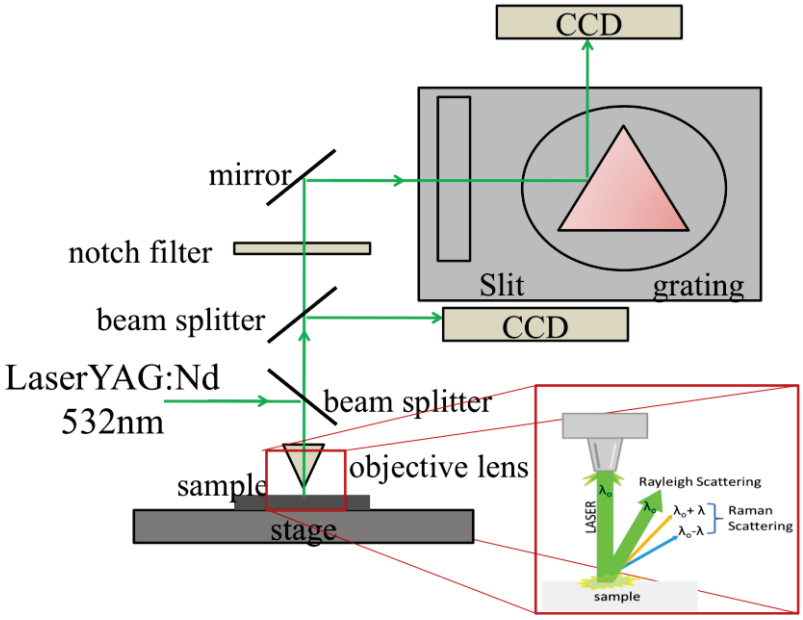

Fig. 6 Raman measurement system

2.3.1-1 Dependence on annealing conditions

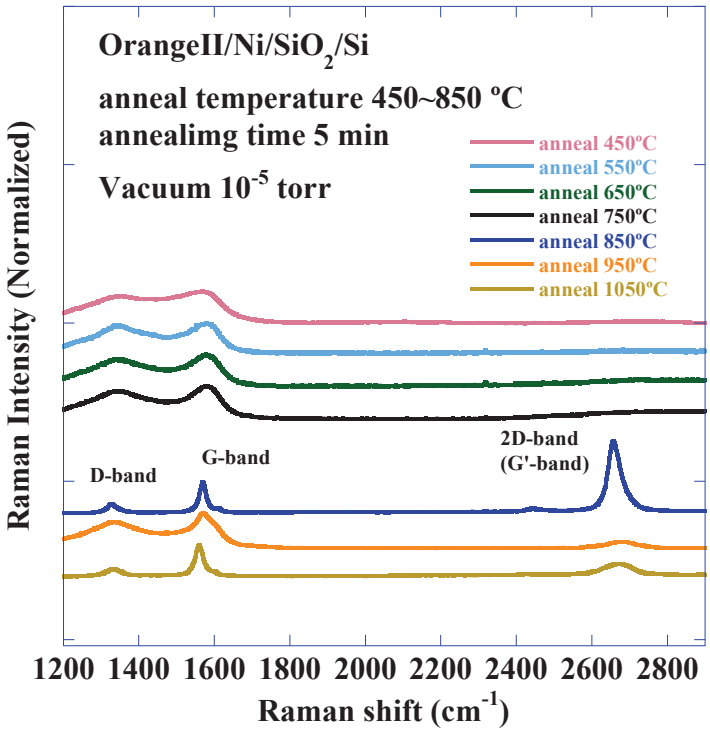

Fig.7 Raman spectra at different annealing temperatures

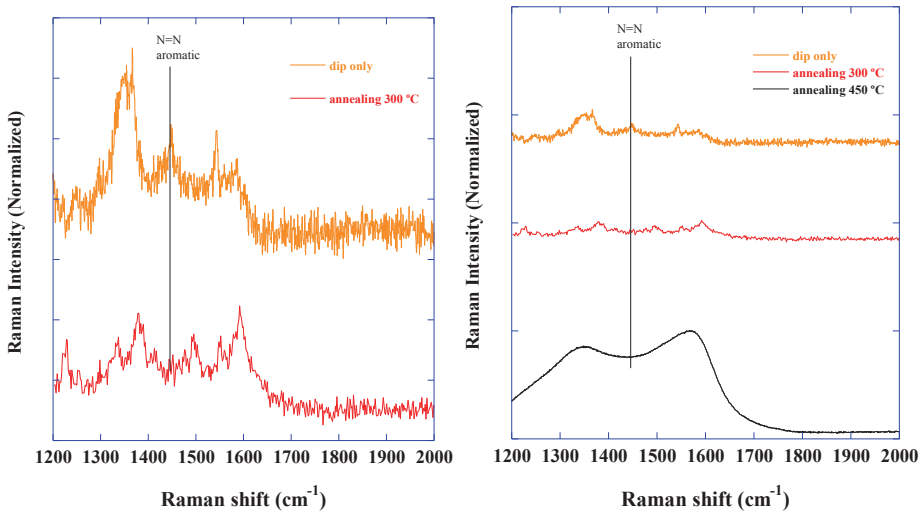

Fig.8 Raman spectra of Orange II before and after heating

Figure 7 shows the Raman spectra of the samples annealed at different

temperatures. The Ni layer was deposited by vacuum deposition. The thickness of the Ni layer was ~100 nm. The samples were annealed under vacuum (better than 10^{-4} Torr) from 450 °C to 1050 °C for 5 min under an IR lamp. Each sample was analyzed, and its spectrum was obtained and normalized with respect to its G-band. The peaks in the Raman spectra for the samples from 450 °C to 750 °C suggest amorphous carbon (a-C). These also imply that the temperature of heat treatment was low, the treatment time was short, or both. Peaks of the D- and G-bands, as well as the G′-band (2D-band), began to appear at above 850 °C, thus confirming graphitization. Raman spectrum of Orange II after heating is shown in Fig. 8 (a). A peak of the azo group at around 1440 cm^{-1} disappeared upon heating at 300 °C, and the shapes of the other peaks are similar. Spectra of compounds such as $C_xH_xO_x$ or $C_xH_xN_xO_x$ may observed in the Raman

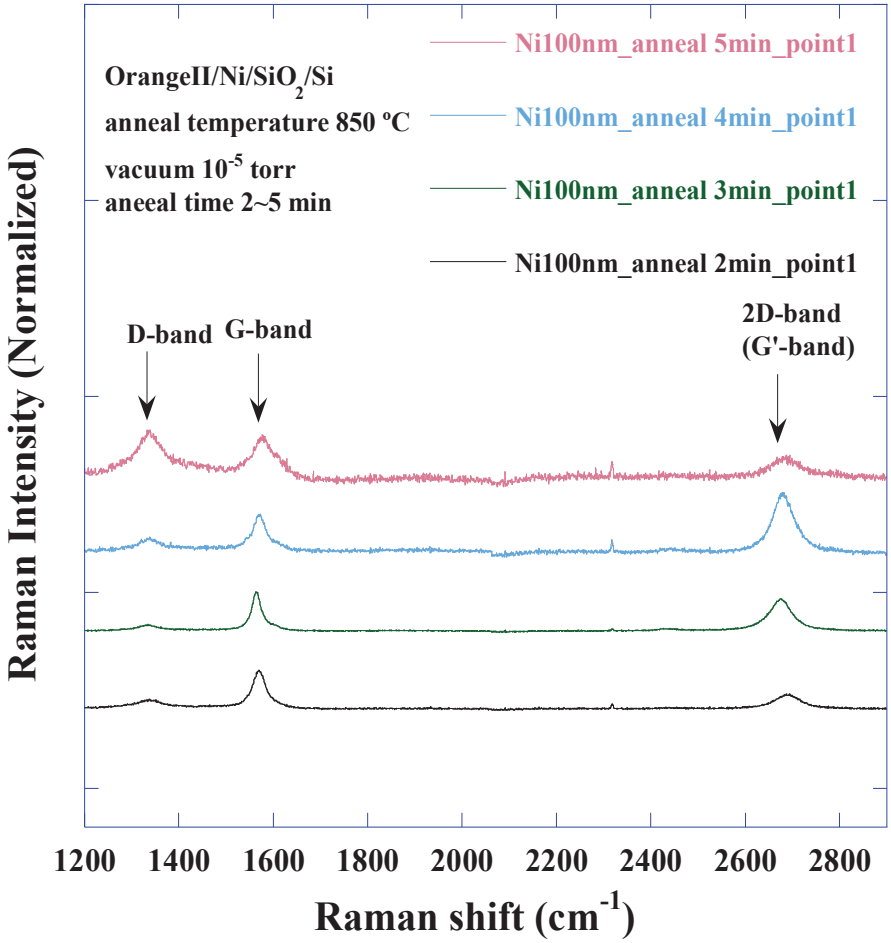

Fig. 9 Raman spectra at different annealing times

spectra. When heating treatment was done higher than 450 ºC, a new peak observed for a-C by Raman spectra as shown Fig. 8 (b).

Next, the dependence on the annealing temperature at annealing times of 2 min to 5 min is depicted in the Raman spectra of samples prepared using a fixed thickness of Ni film (100 nm) and at an annealing temperature of 850 °C (Fig. 9). Although monolayer graphene could not be observed, the 2D-band could be observed in all spectra. This result implies that thermal decomposition of organic matter is sufficient in the process of heating from RT to 850 °C. Although the spectral shape of samples annealed for long periods is sharp, the intensity of their D-band tends to increase simultaneously. This observation may be due to crystal growth of Ni during annealing. Efficient graphene fabrication can be expected by short-time annealing from 2D-band behavior.

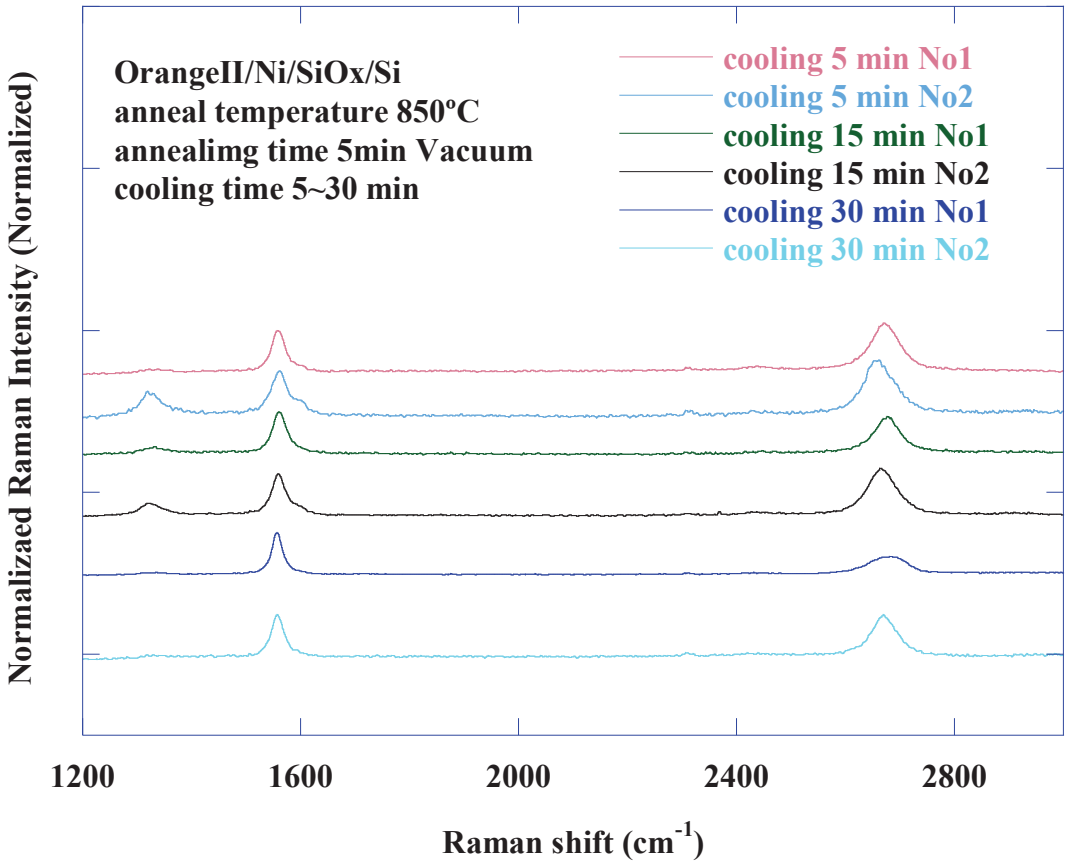

Fig.10 Raman spectra of different cooling time

Then, samples were prepared focusing on cooling time, which is an important parameter related to crystal growth. Figure 10 shows the Raman spectra of samples when cooled to RT by 5 min, 15 min and 30 min on a Ni film of 100 nm thickness. The annealing temperature was 850 ºC and the annealing time was 5 min. The cooling rates were 2.37 ºC /s, 0.91 ºC /s and 0.46 ºC /s respectively. For these samples, could observe a multilayer graphene like spectrum at everywhere. However, as for the crystallinity of graphene, there was not much change only by changing to cooling time as compared with the sample prepared so far.

Finally, the experiments were conducted focusing on the film thickness of catalytic metal Ni. As for sample preparation conditions, Ni was deposited as thick as 20 nm, 100 nm and 250 nm by the vacuum deposition, the substrate surface was coated with Orange II solution stirred with acetone by dip coating, and then, the annealing treatment was performed. The annealing temperature was fixed at 850 ºC, from the result of annealing temperature dependence. Raman spectra for the samples are shown in the Fig. 11. A strong D-band signal of the sample with small thickness (20 nm) could be observed. Also, the peak shape of the G-band was broad. It was confirmed that the peak intensity of D-band became weaker as the film thickness increased to 100 nm and 250 nm. A plot of the G / D ratio of each sample is shown in Fig. 12. There was almost no D-band peak in the sample of 250 nm, and it was confirmed that the crystallinity of graphene and graphite depends on the film thickness of Ni in dip coating. Furthermore, the peak position of 2D-band seems to be influenced by the surface condition of Ni. But, as shown, there is a tendency to get closer to the peak position reported in the literature as the film thickness is increased (black line in Fig. 12). From the results of G / D ratio, domain size was also improved by the Ni layer thickness increasing.

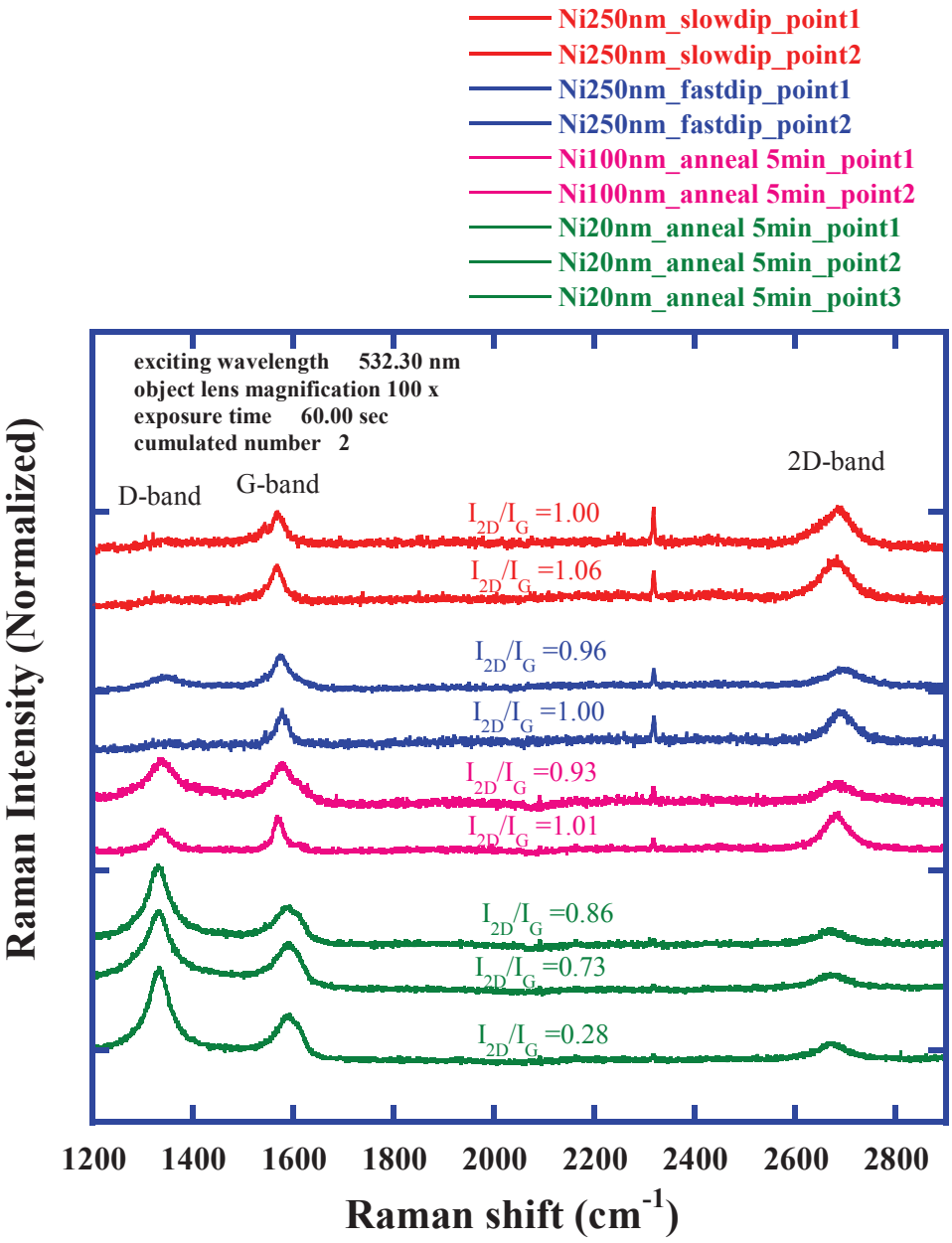

Fig. 11 The graphene formation depended on Ni thickness

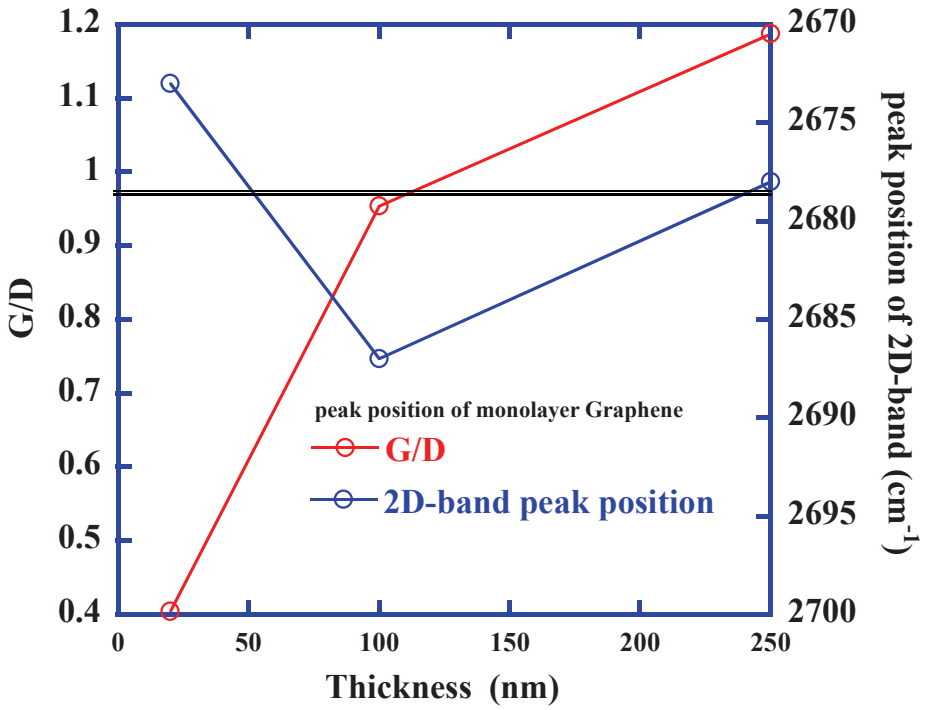

Fig. 12 The relationship of graphene crystallinity and 2D-band peak position

2.3.1-2 Effect of the film-forming conditions on the metal

A Si (100) substrate with an oxide layer of 250 ~ 300 nm thickness on its surface was used as the starting material. After chemically cleaning of the Si wafer, pure Ni was sputtered on the oxide as the catalyst. During the Ni sputtering, the substrate was heated up to 500 ºC and the plasma power was

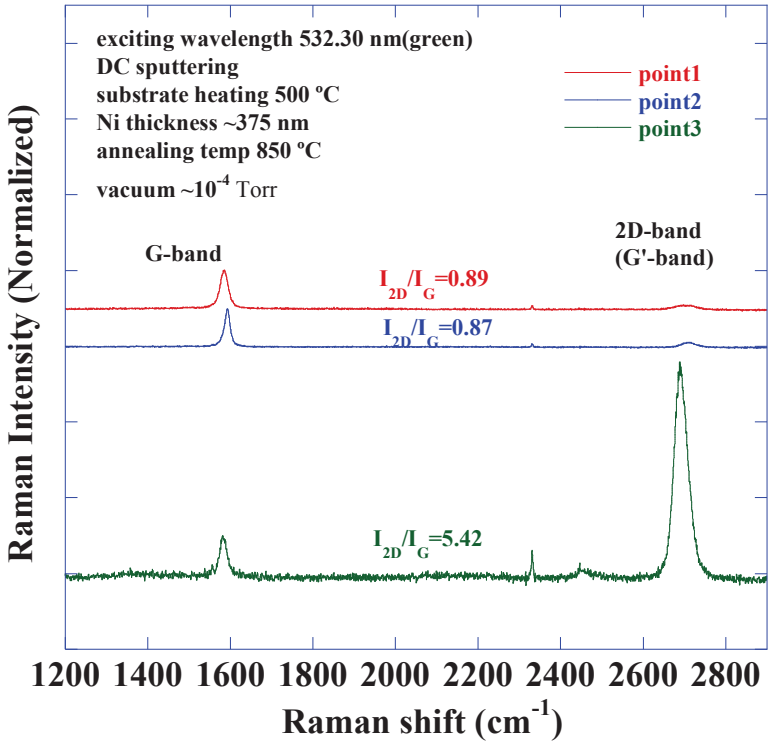

Fig. 13 Raman spectra of sputtering and substrate heated sample.

kept at 150 W. The deposition time was 25 min, while the flow rate of Ar gas was kept at 10.0 ml/min, and the pressure was kept 0.65 Pa, respectively. The sputtering rate was about 13~15 nm/min by this condition. Therefore, the Ni film thickness was 325 ~ 375 nm. Figure 13 shows that Raman spectra of the sputtered samples after dip coating and annealing. Single layer graphene and high crystalline graphite formed at 850 ºC. Raman shift peaks of graphite with few lattice defects and monolayer graphene were observed. Moreover, the grain size of Ni formed by the sputtering was larger than that from vacuum deposition.

2.3.2 Investigation by atomic force microscope

Using an atomic force microscopy (AFM), it is possible to measure topography of a sample surface at a high resolution. This information is gathered by contacting the surface with a mechanical probe called cantilever.

Observation of the sample surface at 850 °C was performed by AFM. The shape image was obtained by extracting only the main component using fast Fourier transform. From this atomic image, the honeycomb structure of graphite and graphene was confirmed. It also

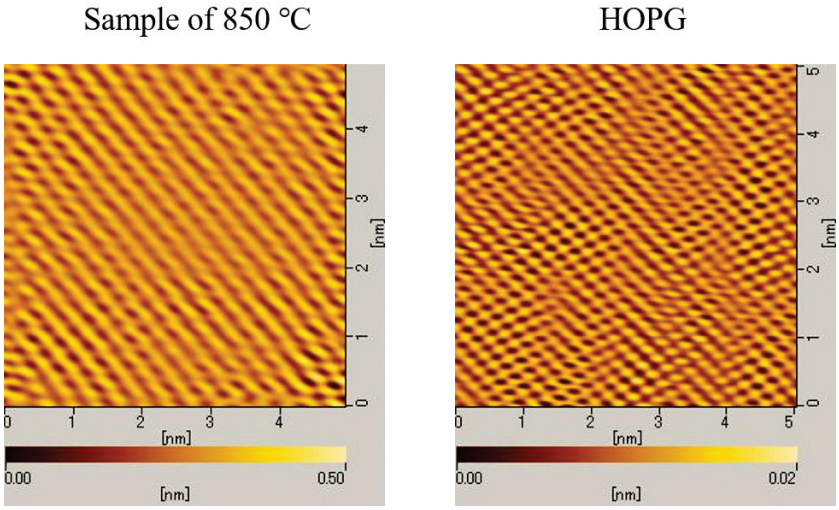

Fig.14 AFM atomic images.

confirmed that the graphite structure had sufficient crystallinity for measurements of the atomic image. The honeycomb structure of the hexagon could observe from the sample made from an AFM image. A commercial graphite (highly ordered pyrolytic graphite, HOPG) sample was used as a comparison. A clear atomic image identical to high oriented pyrolytic graphite surface was obtained as shown in Fig. 14. The totally similar images were obtained. The measuring area was on the top of polycrystalline Ni film, the formation of graphene was strongly suggested.

2.3.3 Observation by scanning electron microscope

Figure 15 (a) is a scanning electron microscope (SEM) image of the sample formed by Ni vacuum deposition, and Fig. 15 (b) the sample is for formed by Ni sputtering. While the sample surface is rough formed by vacuum deposition, the sample formed by a sputtering is seen as quite flat. When a film was formed by a sputtering, the grain size of Ni was large than that of deposition, and the surface roughness decreased. The samples of graphene and graphite with larger size are considered to be related to grain size of Ni. Even if annealing was done for the sample formed by vacuum deposition, the grain size was still small, and the surface was rough too.

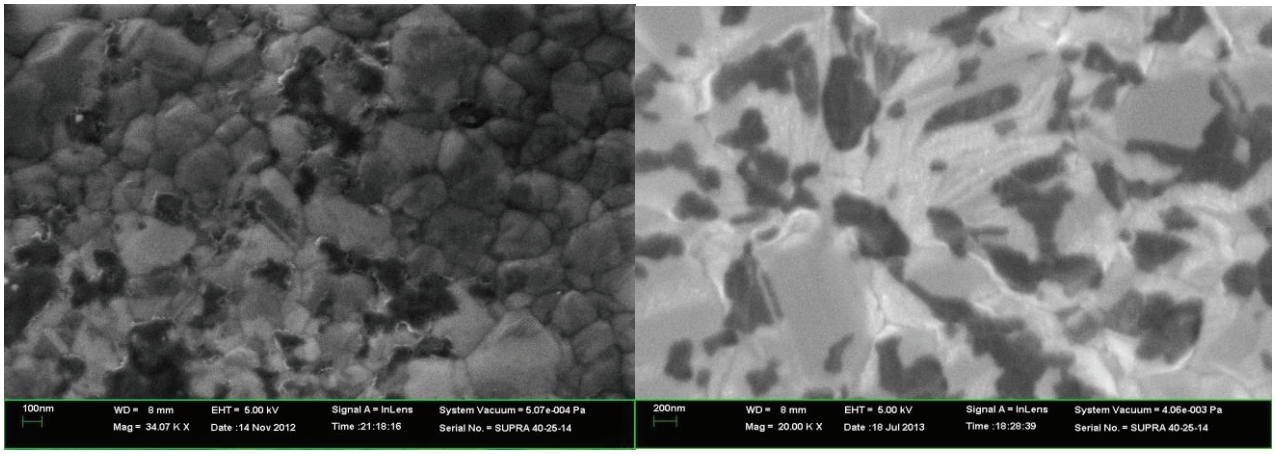

(a) (b)

Fig.15 The sample surface SEM images of (a) Ni vacuum deposition and (b) Ni sputtering with substrate heating at 500 °C

2.3.4 Investigation by X-ray diffraction

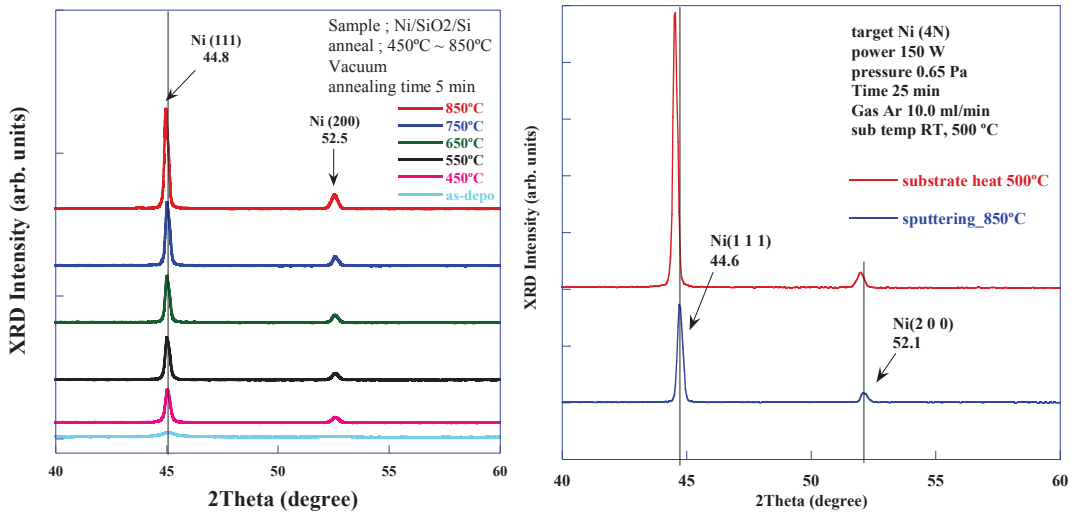

(a) (b)

Fig. 16 XRD patterns of Ni thin films formed by (a) vacuum deposition and (b) sputtering

The X-ray diffraction (XRD) pattern of the Ni layers formed by vacuum deposition and by Ni sputtering were indicated in Fig. 16. All samples in Fig. 16 (a) were deposited without substrate heating and measured after annealing from 450 °C to 850 °C by a step of 100 °C. The Orange II was not coated on these samples. The XRD peak could not be observed only by the deposition at RT, however, Ni did a crystal growth by annealing at 450 ºC and higher temperatures, and Ni (111) and (200) XRD peaks were growing. On the other hand, as shown in Fig. 16 (b) for the sample made by Ni sputtering without substrate heating, the XRD peak intensity was strong like the vacuum deposited sample even for substrate temperature of RT. However, the Ni (111) peak became strong and shifted to the low angle side by sputtering Ni with in substrate heating at 500 °C. The grain size of the samples was estimated from the Ni (111) peak using Scherrer equation (2.3.1):

$$D = \frac{K\lambda}{B\cos\theta} \qquad (2.3.1)$$

Here, D is the grain size, λ is the X-ray wavelength (Cu Kα 1.5418 Å), θ is the diffraction angle, K is the Scherrer constant and B is the peak of full width at half maximum (FWHM), respectively.

The Ni grain size of sample formed by vacuum deposition was about 200 nm, the sputtering with substrate heat at 500 °C was about 1 μm. Even there was no organic coating, small graphene spots were also grown on some Ni grains. The carbon source might come from the impurity in Ni metal. The graphene size, however, was different for Ni sputtering and vacuum depositing samples. The graphene size of Ni sample was about five times larger than that of the deposited Ni sample one. So, a large Ni facet is important in large area graphene growth.

2.3.5 Investigation by X-ray photoelectron spectroscopy

The sample produced by the above-mentioned process and graphene samples produced by CVD or peeling from highly ordered pyrolytic graphite (HOPG) were measured by X-ray photoelectron spectroscopy (XPS). (A ration of the ingredients of sp^3 with sp^2 was analyzed.) Since the various carbon states exists in the range where x-ray has irradiated, a broad peak was obtained from sample of orange II, as shown in Fig. 17 (a). A monolayer graphene sample showed sharp and strong peak at 284.6 eV. A relative broad peak was observed for multilayer graphene sample. In addition, we show the XPS spectra of C1s orbits of four samples in Fig.17 (b). It is shown that our sample was more like the multilayer CVD one. The sp^3 peak of C1s orbits was also observed from the monolayer graphene, which was considered to come from the unevenness of the graphene sheets. Although our sample had more grain boundaries, the spectrum of the multilayer like graphene was obtained. Since our samples were formed from organic solution, an OH bonded C peak could be seen in the XPS result. As shown in Fig. 18, furthermore, residual sodium (Na) and sulfur (S) were also observed in the XPS measurements. However, nitrogen (N) could not be observed in XPS spectra. As using Ni as growth catalyst, the signal other than Ni and C were also observed in the XPS measurement. For the Ni sputtering XPS spectra, Ni oxides (NiO, Ni_2O_3), sodium (Na) and sulfur (S) could be recognized, as shown in Fig. 18. The nitrogen (N) signal was not detected. These impurities might come from the Orange II solution, this also gave rise to a possibility of doping in graphene.

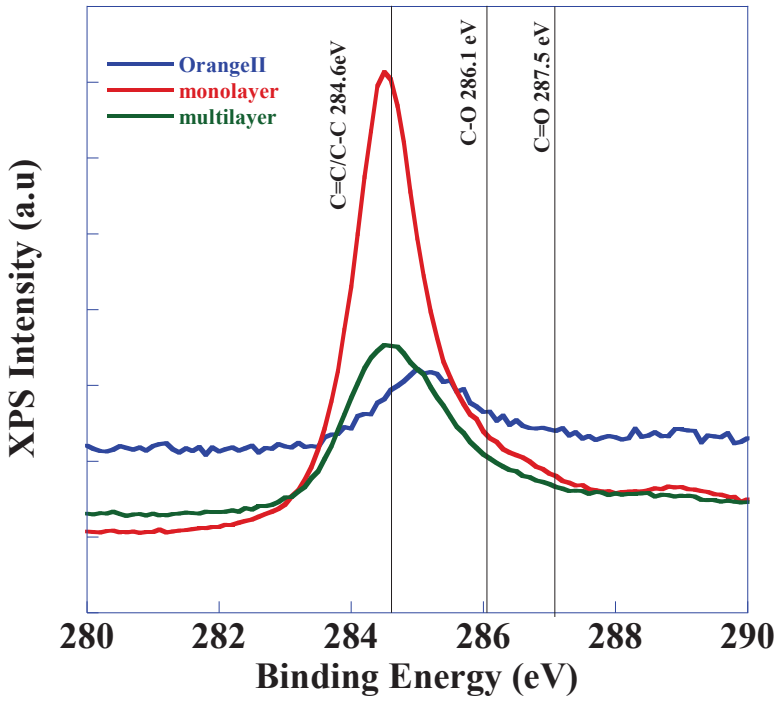

(a)

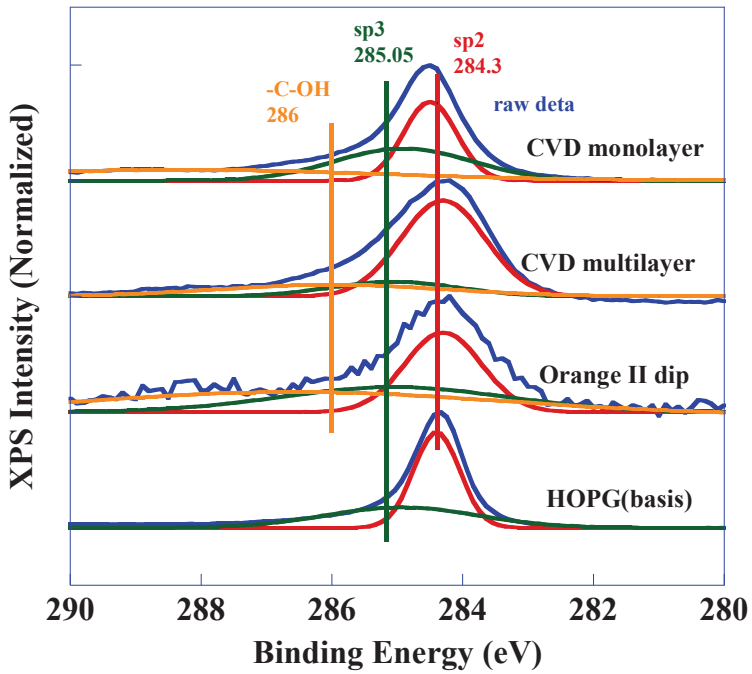

(b)

Fig. 17 XPS spectra of (a) C1s orbital raw data and (b) fitting results of each sample

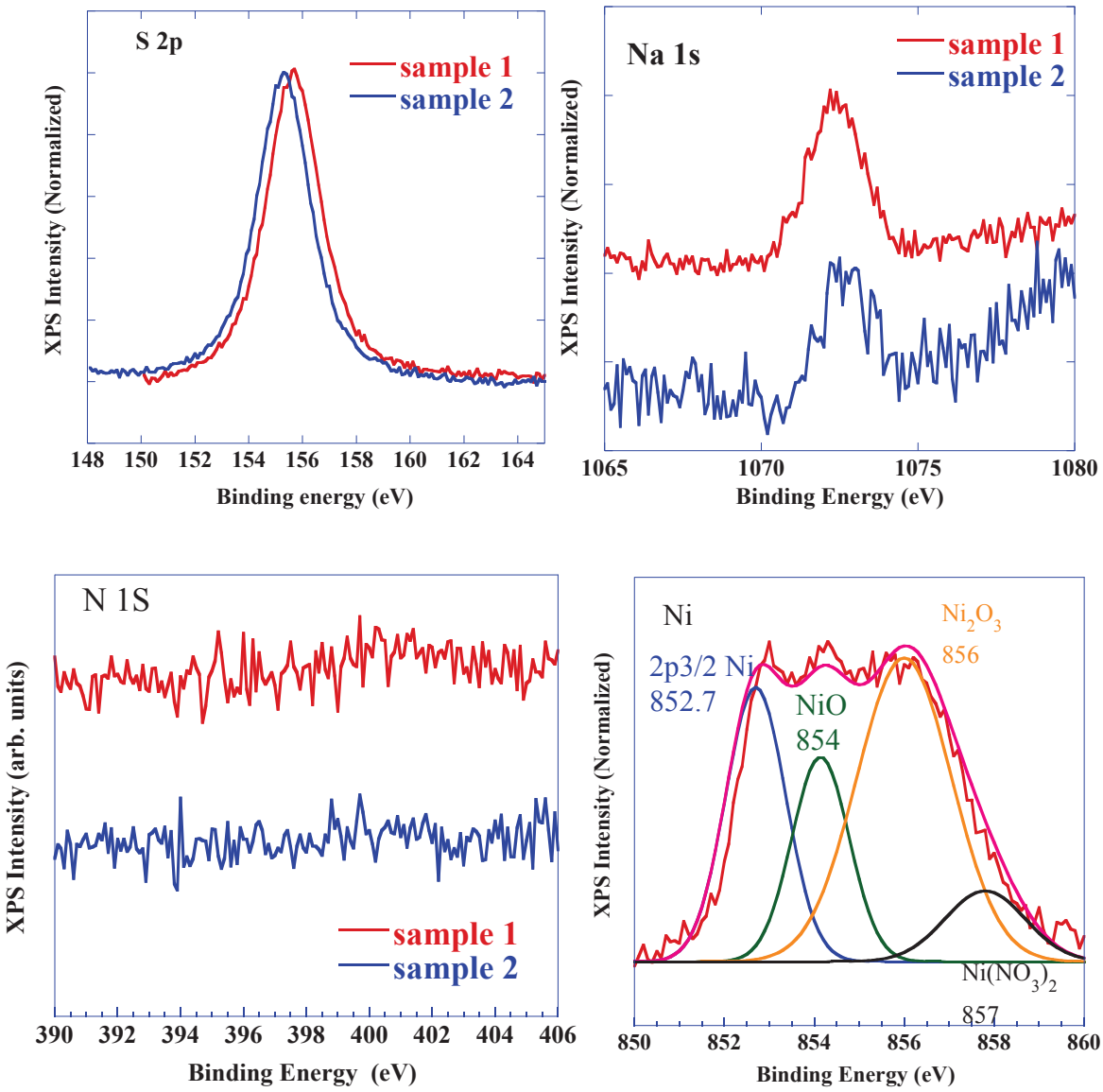

Fig. 18 The XPS spectra of elements other than carbon from Orange II coated graphene sample

2.3.6 Growth mechanism

The lattice constant of graphene and the lattice constant of Ni (111) are very close, correspond to the possibility graphene growth on the Ni (111) grain facet. The graphene nucleus is first formed on the facet and a grow-up to large area graphene sheets. Thus, we could observe single layer graphene by Raman spectra. The carbon resource, the graphene nucleus, all of the necessary things could be provided by the pyrolysis of Orange II, which dissolved in to the Ni catalyst and formed nucleus on the Ni facet during a cooling process from 850 °C. When the azo group was pyrolyzed N_2 and radicals were generated. The radicals pulled out hydrogen and cyclized, so Orange II split into the naphthalene ring part and the sodium benzenesulfonate side by this. In addition, C-H, C-C bond might cleave to form reactive free radicals, cause molecular rearrangement, aromatic condensation, elimination of side chains, even all these processes could occur in parallel during carbonization [43,44]. It can be considered as follows

$$2\ (C_{16}H_{11}N_2NaO_4S) \rightarrow C_{30} + Na_2S_2O_3 + 5H_2O + 2CH_4 + 2N_2 + 2H_2$$

Polymerization at the most reactive 1-position leads to naphthalene polymers which can form full condensed polymers composed of only six-membered ring, while polymerization utilizing the less reactive 2-position can inhibit condensation. These factors are thought to affect the crystallinity of graphene by using Orange II organic solution. In addition, methane generated by thermal decomposition in the vicinity of the surface of the metal reacts with the metal, and it is dissolved into the Ni, so it is thought that nucleation on Ni grain grows to relatively large graphene.

Graphene growth by organic matter dip coating could be produced even on Ni patterns. It provides a possibility of wiring the graphene due to its growth process. Moreover, since the element which constitutes the organic matter remains in the substrate, the characteristic of graphene may be changed easily.

Summary

As described in chapter 2, graphene and graphite thin films were fabricated by coating with an organic solution and post-annealing using a very simple and quick method. The results of Raman spectroscopy reveal a strong dependence on annealing temperature beyond 850 °C and localized generation of single-layer graphene. On the basis of these results, the temperature was fixed and both the annealing and cooling times were varied to improve the size and crystallinity of graphene. However, the intensity of the D-band changed little despite long annealing of the sample. The intensity of the D-band was dependent on the crystal growth of Ni grains; greater Ni film thicknesses tended to reduce the intensity of the D-band signal. Cooling time also seemed to be an important factor and was thus examined experimentally. Moderate cooling changed the 2D-bands but did not fundamentally improve them. The dependence of Ni on film thickness was apparent because heating and cooling treatments could not improve the crystallinity of graphene with use of the Ni catalyst. The D-bands weakened, as in case of the samples with thick Ni film. When the film was formed by sputtering on a substrate heated at 500 °C, D-bands for graphene almost could not be observed in the Raman spectrum of graphite. When sputtering and substrate heating were performed at 500 °C, Raman spectra of graphene and graphite with almost no D-band were obtained. This result is due to the preferential growth of Ni (111), the smaller difference between the period of the surface lattice and the lattice constant of graphene, as well as the formation of an epitaxial film. The surface roughness disappeared and the grain size became larger compared with those of the film formed by vacuum deposition, thus including the growth of graphene and graphite of a certain size in two dimensions.

Chapter 3. In-situ observation of graphene growth by an optical microscope

We succeeded in fabricating graphene from organic matter as it was written at the previous chapter. So, we were considered in order to observe the state which from organic matter changes into graphene. In this section, we present observation method of graphene by using in-situ optical microscope propose by our group.

3.1 Observation systems

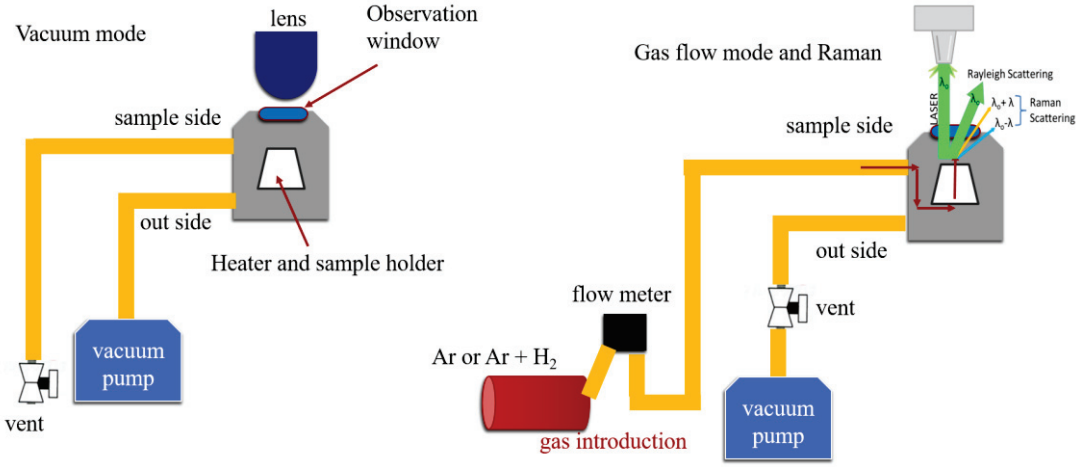

(a) (b)

Fig.19 In-situ observation system (a) vacuum condition and (b) observation of gas flowing condition with Raman measuring at different temperatures

An optical microscope instrument, the KH-7700 (Hirox), was used for in-situ observation of graphene growth. The objective lens magnification is in a range from 140 to 1400 times. The light source is a metal halide lamp. The heating stage for observation is set in a vacuum chamber (S.T. Japan Co., Ltd), as shown in Fig. 19. The main features of the system are temperature range from room temperature (RT) to 900 ºC, the ultimate vacuum of 1 x 10^{-6} Torr and the maximum sample size of 10 x 10 mm^2. The

optical observation and in-situ Raman measurements were performed through a quartz window of the chamber. The 532 nm (Nd-YAG) laser was used for exciting the Raman scattering.

3.2 In-situ optical microscope observation

The samples for the in-situ observation were two tapes, one was formed by Ni sputter deposition on the Si substrate, as shown in the previous chapter, and the other was on a pure Ni foil. First, a result for the samples formed on the $Ni/SiO_2/Si$ substrate is indicated in Fig.20 (a). The temperature rising method was different from the previous chapter, this samples were heated from RT to 850 ºC. The image was first recorded at RT, an characteristic color of Orange II could be seen. Then the sample was heated and images were taken for every 100 ºC from 450 ºC which is the temperature organic matter pyrolyzes. Pyrolyzes of an azo group is going at higher than 400 ºC, and the characteristic color of Orange II disappeared. When the heating was continued, a blue part appeared on the Ni surface. The color became dark after that, and a change with the color was also observed besides the blue region. Raman spectra of a heated sample were measured at RT and shown in Fig 20 (b). G-band and 2D-band corresponding to graphene could not be observed at every point (1~5) from this in-situ observation area. However, the same $Ni/SiO_2/Si$ sample heated by using an IR lamp gave rise to G-band and 2D-band signals, as shown in Fig. 20 (b) with the blue line spectrum. It is thought that since the heating by the OM system's heater, the heat transfer was not good by the Si substrate. Also, it might have a problem of adhesion between the Si substrate and Ni thin film. Raman measurements were also performed on the Si substrate, but a sharp spectrum like graphene could not be observed although a spectrum like charcoal was observed.

The heating behavior of the sample of Orange II coated Ni foil is shown in Fig. 21. As shown in Fig. 21 (a), the original orange color of Orange II disappeared at temperatures higher than 450 °C, indicating the organic matter pyrolying on the Ni surface. For heating at 850 °C and 5 min, a growth of Ni grain could be recognized. However, the growth of graphene could no be observed clearly. After cooling the sample to RT, Raman spectroscopy was carried out at some random point of the sample surface. As shown in Fig. 21 (b) a graphitization procedure and a carbon derived peak were observed. In contrast, there are no clear graphene related peaks observed. For this sample, a temperature dependent Raman was also measured, as shown in the observation system in Fig. 19 (b).

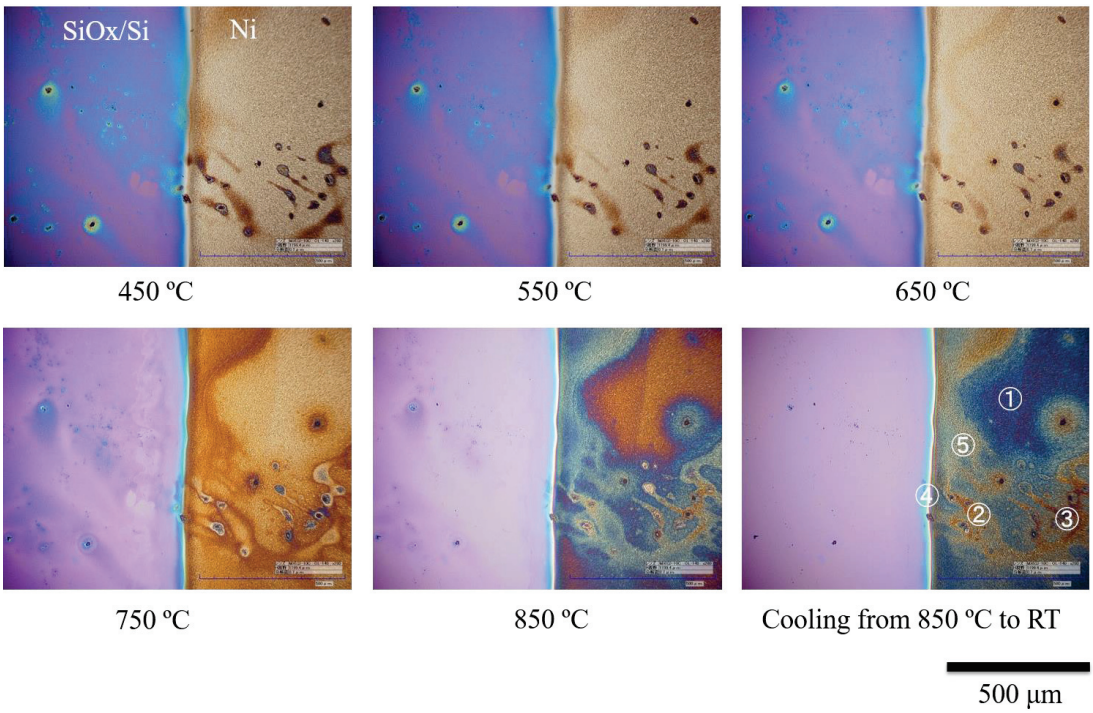

(a)

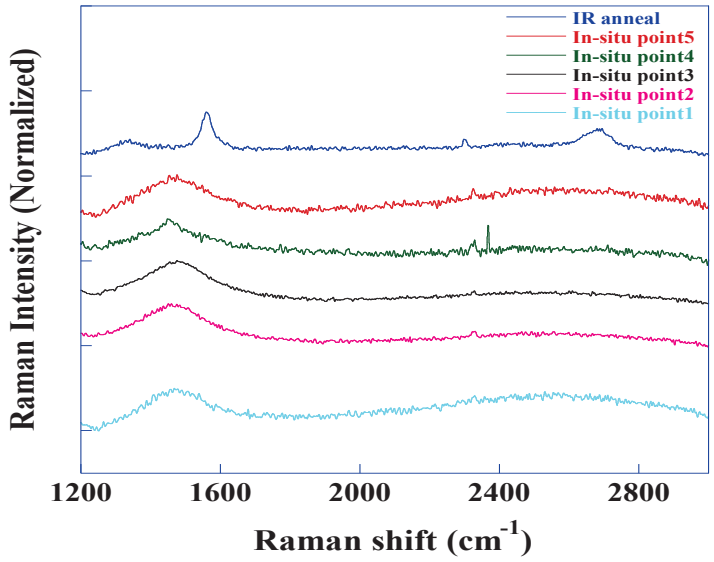

(b)

Fig. 20 OM images of Ni deposited on Si substrate samples and Raman spectra

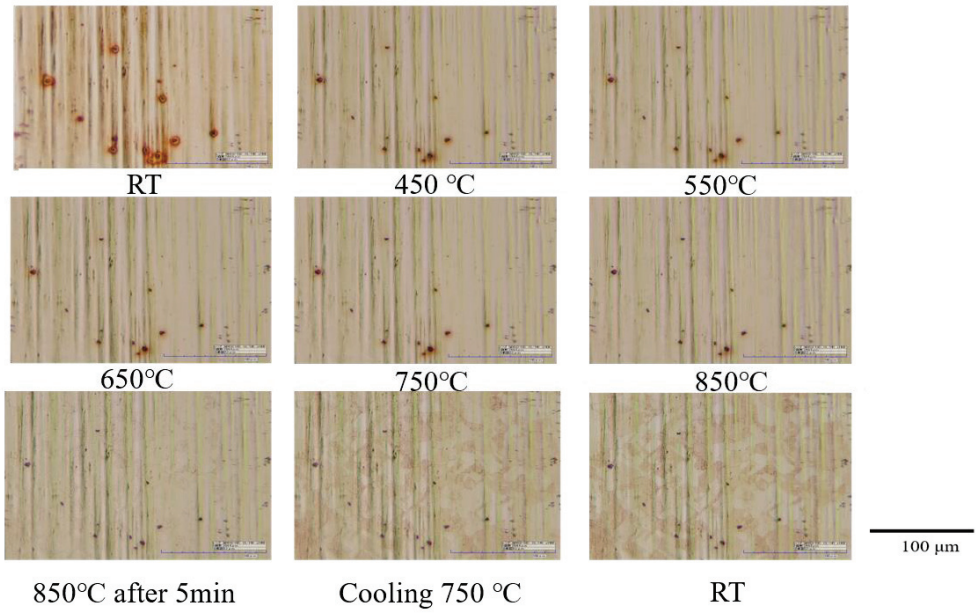

(a)

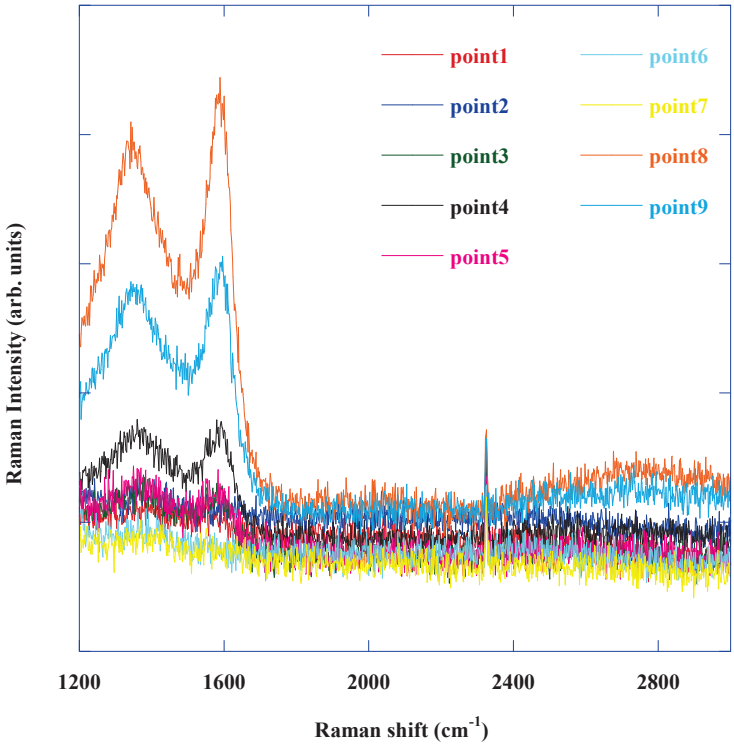

(b)

Fig. 21 OM image of Ni foil sample and Raman spectra

3.3 In-situ Raman measurement

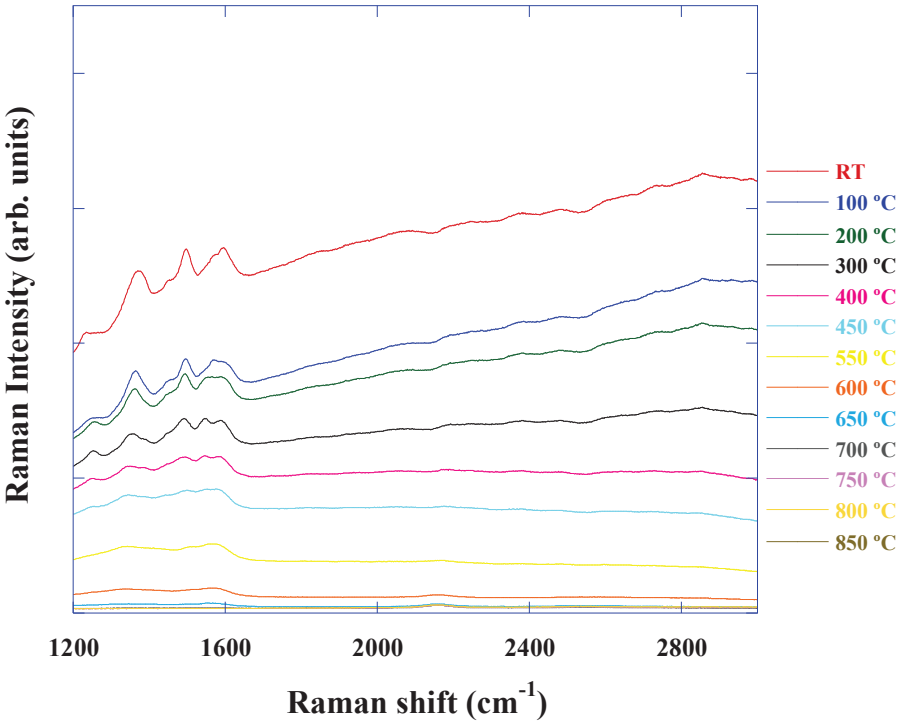

Fig. 22 In-situ heating Raman spectra

Figure 22 shows Raman spectra of in situ and heating Raman. The measurement conditions were excitation light 532 nm, integration time 1000 ms and average number of 30. The measurements were taken at the area where Orange II existing. At temperatures lower than 450 °C (lines red to light blue from upside Fig. 22), typical Orange II like Raman peaks were obtained. The organic matter was pyrolyzing at this temperature. After that, amorphous carbon like Raman peaks were recorded for temperatures of 550 °C to 850 °C. Unfortunately, these was no clear graphene like peak in the Raman spectra. This is the manner different from Orange II coating and IR annealing. The reason is not clear, but a higher temperature like 900 °C or a large Ni grain might be necessary to form evident graphene while large part of amorphous carbon existed.

3.4 In-situ observation of fabricated CVD graphene on metal

In order to observe how organic matter grows to graphene, multilayer graphene was prepared on Ni by using CVD. This sample was heated in vacuum and observed with the optical microscope. The temperature was raised from RT to 900 °C. Picture were take a at different temperatures. In the previous research, they used an electron microscope to observe with graphene on Ni [45]. Dissolving and regrowth of graphene are observed using the carbon layer deposited Ni by heating and cooling. According to the previous work, graphene dissolves at ~ 900 °C or higher, and a monolayer graphene segregates at ~790 °C to 900 °C on the Ni (111) surface [46]. If this behavior can be observed with an OM, it is possible to observe the growth of graphene on the Ni by this easy way. The experiment was conducted by changing the rate of rising temperature.

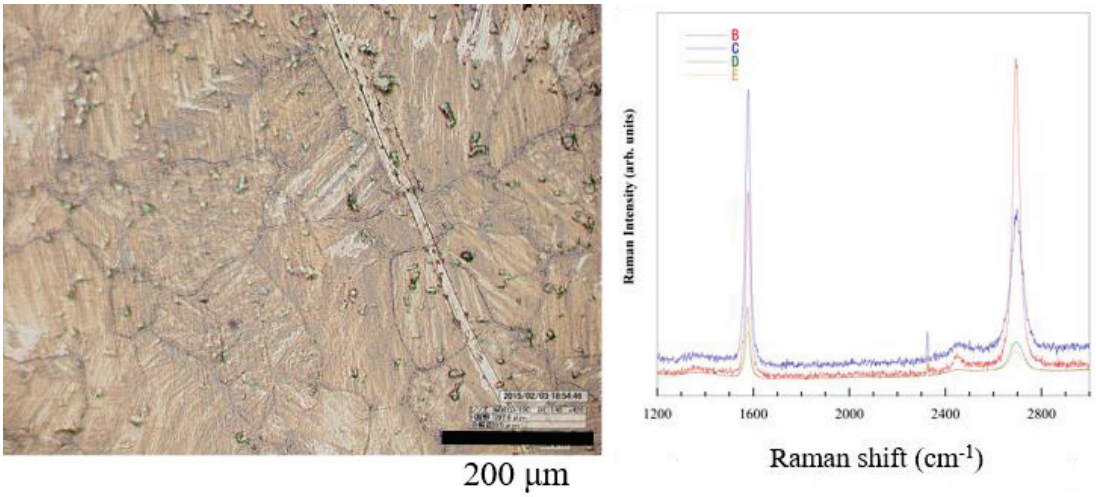

(a) (b)

Fig. 23 (a) OM image of CVD graphene on the Ni foil, (b) Raman spectra of Ni foil sample

3.4.1 50 ºC/min rising rate

A sample of multi-layer graphene fabricated on Ni foil was prepared by ethanol chemical vapor deposition (CVD). Afterwards, the sample was heated at 900 ºC in the vacuum chamber using the OM system's heating stage. This high temperature was enough to dissolve the segregated

graphene layer, then a monolayer graphene was grown by controlling the temperature between 800 ~ 900 ºC. The pressure of the vacuum was about 10^{-5} ~ 10^{-6} Torr. Figure 23 (a) shows the OM image of this graphene/Ni sample. The sample surface was covered by monolayer and/or multilayer graphene. The light color areas were almost monolayer graphene ones. Fig. 23 (b) shows the Raman spectra randomly taken from four points on the sample surface. Monolayer-like (red line) and multilayer-like (others) graphene signals were confirmed. Afterwards, the sample was heated to 900 ºC. At this temperature, the graphene was dissolved and immersed in Ni metal, as shown in Fig. 24 (a). A naked Ni surface was observed. It was confirmed that some carbon condensed areas developed on the Ni surface, as shown by the thick color spots in Fig. 24 (a). These areas were amorphous carbon (a-C) condensation, which could be seen in all of the OM images in Fig. 24. In the next step, we decreased the sample temperature to 800 ºC, and took the OM image as Fig. 24 (b). Color changing was seen on the Ni surface, suggesting graphene formation. Then, the sample was heated to 900 ºC again, took the OM image, and re-cooled down to 800 ºC. This cycle was repeated by several times. Fig. 24 (c) to (e) are the OM images after heating for 2 to 5 times, respectively. The carbon commendation areas grew with the heating – cooling cycles. Finally, the sample was cooled down to RT, which is shown by the OM image in Fig. 24 (f). The sample cooled down to RT from Fig. 24 (e) was carried out by Raman point spectroscopy. The picture taken from large area of the sample is shown in Fig. 25 (a). The Raman spectra taken at the points 1 ~ 14, which were indicated in the image. The Raman spectra were shown in Fig. 25 (b), (c) and (d). Based on those spectra, it was confirmed that graphene layer was re-grown on the Ni surface. The points 1, 2, 7, 8, 12, 13 were multilayer graphene areas. The points 6, 14 were thin graphene layers. The points 3, 4, 5, 9, 10, 11, in contrast, were amorphous carbon areas. As a result, we found out that it has the various colors in the OM image, which indicate the different layer thickness. Furthermore, the amorphous region is hardly dissolved in Ni at 900 ºC. The formation of big carbon clusters gave rise to the thick blue and orange areas. The occurrence of these condensed carbon clusters is also an obstacle of graphene growth. Thus, a flat Ni (111) surface is important in large graphene sheet growth.

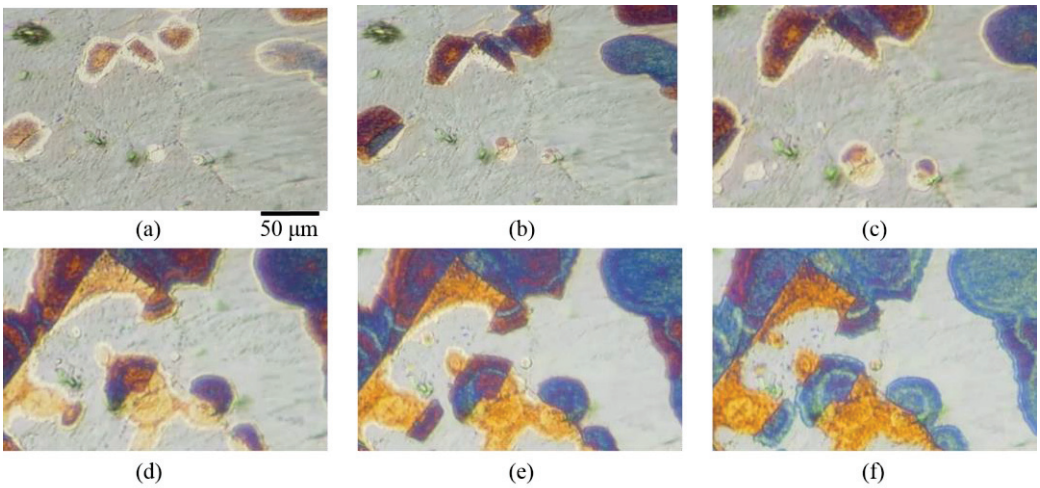

Fig. 24. (a) Image of the graphene/Ni sample heated at 900 ºC. (b) Image taken at 800 ºC. (c) rehated to 900 ºC from (b). (d) cooled down to 800 ºC and reheated to 900 ºC two times from (c). (e) cooled down to 800 ºC and reheated to 900 ºC from (d). (f) cooled down to room temperature from (e).

(a)

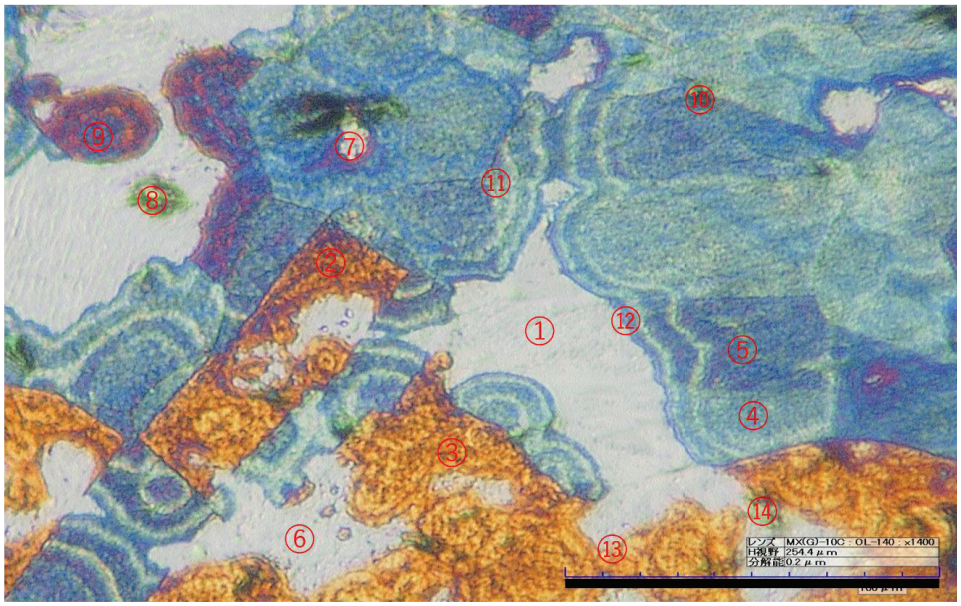
⑨
⑦
⑩
⑪
⑧
②
①
⑫
⑤
④
③
⑥
⑬
⑭

100 μm

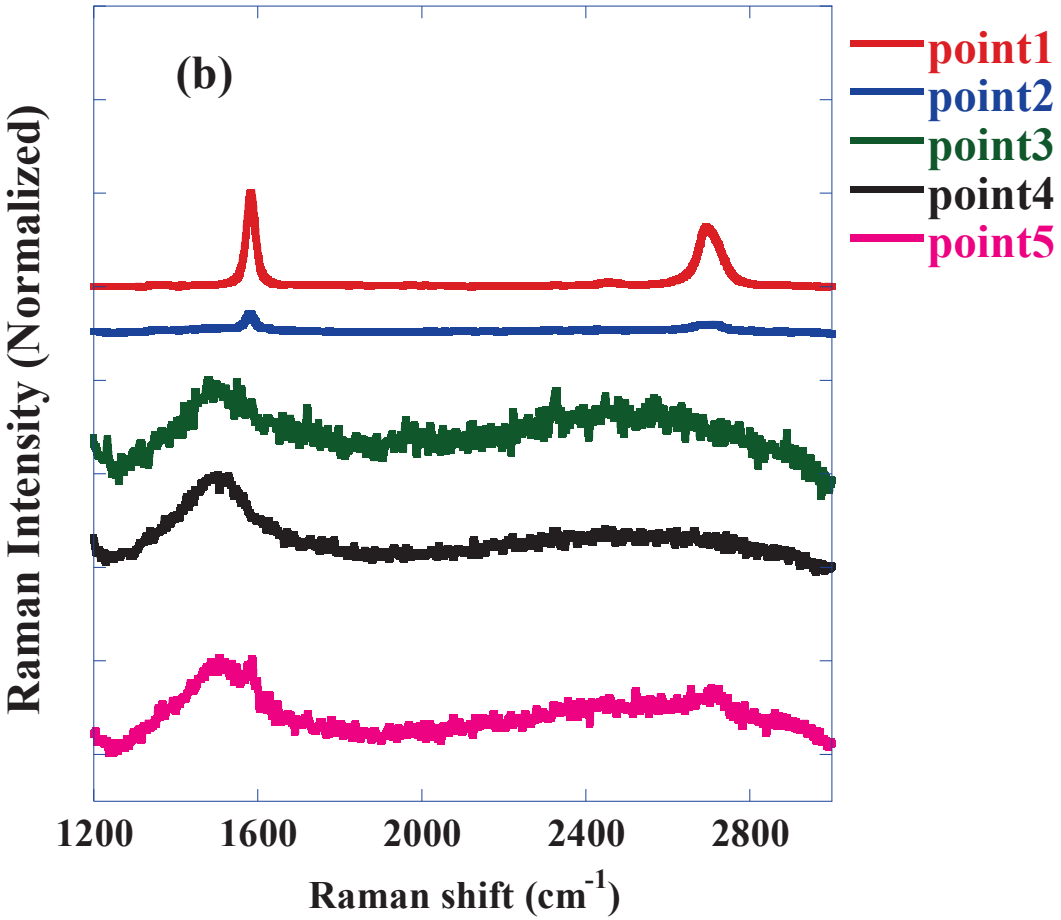
(b)
point1
point2
point3
point4
point5
Raman Intensity (Normalized)
1200
1600
2000
2400
2800
Raman shift (cm-1)

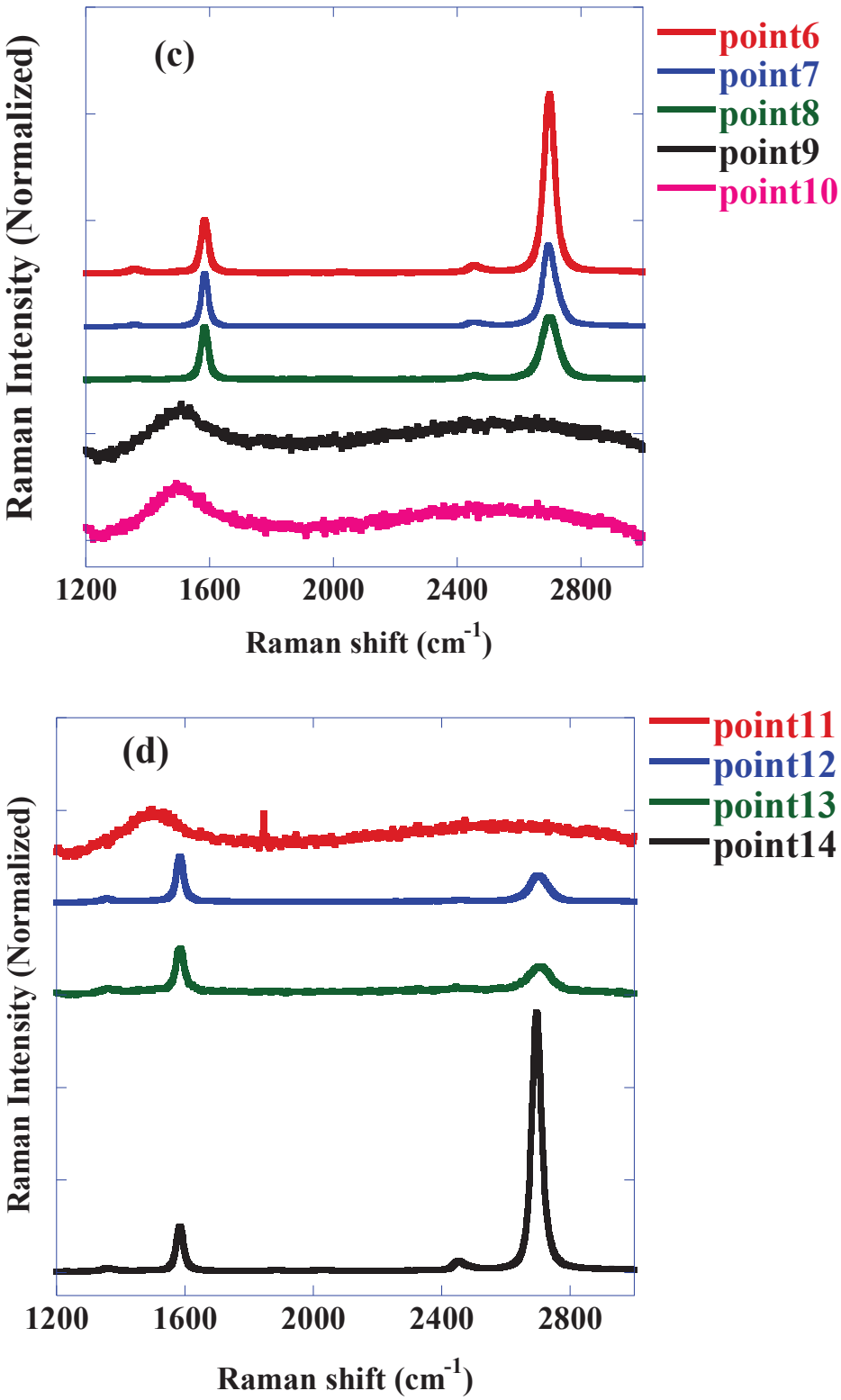

Fig. 25. The measurement location (a) of the Raman spectrum and the spectra, (b), (c) and (d).

Here we can summarize the effects of heating process. The sample surface image shows that the naked Ni surface was obtained at 900 °C. The graphene layer was immersed into the Ni layer. When the temperature was reduced to 850 ºC, the graphene (the white area) and the amorphous carbon (a-C) (the dark blue and orange area) appeared on the Ni surface. By reducing the sample temperature to 800 ºC (in Fig. 24 (b) and (d)), both the a-C and graphene area grew larger. There are also some green points, such as one in the upper left corner in Fig. 25. This is also thin graphene layer, which is grown on a Ni grain.

From the results of Raman, the optical image of the reflectivity a few layers graphene will be looked like light pink area. Figure 26 shows

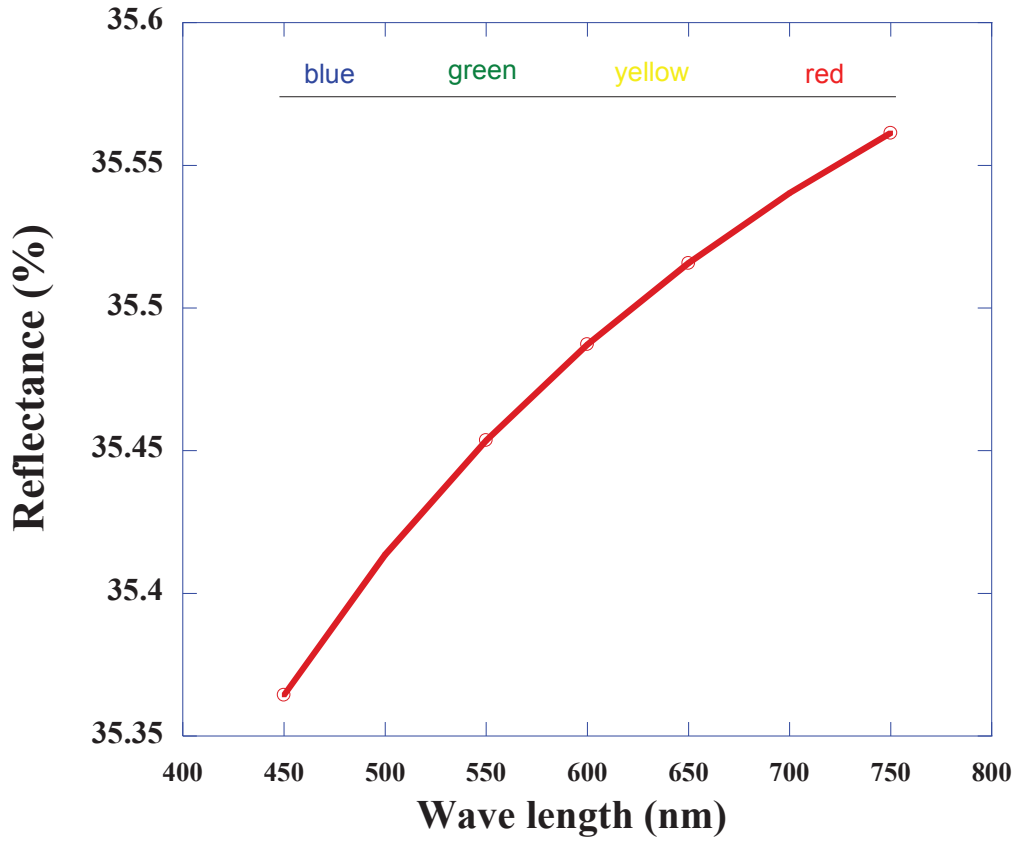

Fig. 26 The calculated reflectivity of single layer graphene on Ni surface.

the calculated reflectivity of monolayer graphene on Ni surface. From the result, we could assume the surface color while heating the sample. The

optical parameters used were refractive index: the air n_0=1, graphene n=2.6-1.3i [47,48] and Ni n_m= 1.75-3.19i (wave length 539.1 nm), respectively. Single layer graphene thickness is d=0.34 nm. In Fig. 26, we show the calculated reflectivity of a single layer graphene on the flat Ni surface. An almost white or light pink color will be seen with the optical microscope for the graphene area. The reflectivity will be slightly changed at high temperatures (800 ºC and 900 ºC), in which the graphene growth is still recognizable by the optical microscope. Graphene growth (regrowth) can be observed using this wavelength difference. In the same calculation, the reflectance in the case of a metal without graphene was 34.7% at room temperature (RT). By changing the sensitivity of detector or optical system we may detect this slight difference, that means the existence of graphene on the metal might be confirmed by the color change of the surface. However, in actual samples, it is difficult to judge from surface irregularities and thermal radiation light. The in-situ observation of graphene growth by the optical microscope is simple and effective. Figure 27 (a) shows the OM image of a re-grown graphene/Ni sample at RT. The large pink area was covered by single or multilayer graphene. The change on the uniformity of color should come from the surface roughness of Ni. The rectangle area in the image was measured by Raman mapping. The lower picture of Fig. 27 (a) shows the mapping results. The bright spots in the lower picture of Fig. 27 (a) reflect the area of single layer graphene, which is shown by the Raman spectrum (high) in Fig. 27 (b). In the present situation, all spectra were obtained when Raman spectroscopy was measured. Therefore, this slight color change is came from graphene.

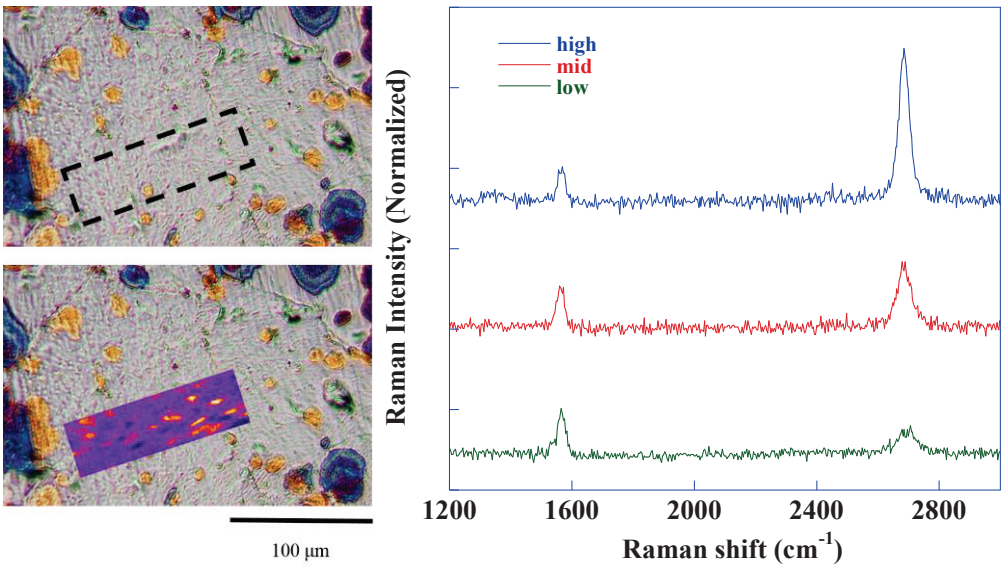

Fig.27 (a) Optical image, where the Raman mapping area indicated by the dotted rectangular line. (b) Raman intensity in the rectangular area.

3.4.2 20 °C/min rising rate

The stating sample was also a CVD grown graphene on the Ni surface. The light color areas were almost monolayer graphene, such as the area I in Fig. 28 (a). This picture shows the in-situ observation OM image taken at RT. From Fig. 28 (b) to (h), the temperature was raised from 400 °C to 900 °C. There was no significant change of the sample surface for temperatures from RT to 600 °C. The color of the sample changed from 650 °C at area I. At temperatures higher than 750 °C, the area started to change to dark color gradually as shown by Fig. 28 (d) to Fig. 28 (h). There is no further change for the area I from 850 °C, but more color changes occurred at area II and III. When the temperature increasing to 900 °C, graphene on the Ni foil dissolved into metal as the in-situ observation by SEM, which could be recognized by the white-green area of bare Ni around area I, as show in Fig. 28 (h). However, the dark color lines and areas kept no change even

keeping the temperature at 900 °C for 5 min, as show Fig. 28 (i). In the next step, we decreased the sample temperature for regrowing of graphene on the Ni surface. Figure 28 (j) shows the OM image taken at 850 °C. The light green color areas occurred at the bare Ni surface near the black spots, indicating the regrowth of graphene by the temperature decreasing. The black area, however, kept as no change both in color and size. Also, the light green areas kept almost the same shape from 790 °C to 500 °C, and RT, as shown in Fig 28 (k) and (l). These facts suggest that the regrowth of graphene mainly took place at temperature range from 900 °C to 800 °C. As described below, the formation of multilayer graphene was confirmed for these light green areas.

There is a difference between Fig. 28 (k) and (l), which were taken at 790 °C and 500 °C, respectively. Figure 28 (l) shows more green thin lines on the Ni facets, but the color besides these lines was white or light pink and exhibited no significant change from Fig. 28 (k). We believe that the single layer graphene was formed at these areas, even we could not confirm it only by the color change of the OM image.

Figure 29 shows (a) the OM image and (b) Raman spectra of the graphene sample after heating in vacuum and cooling to RT. The orange and dark blue areas, such as point 1(red circle area) showed amorphous like carbon singles. The light color areas such as point 2 (blue circle area) showed multilayer like graphene Raman spectra. There is also monolayer-like graphene area, such as point 3 (green circle area). These graphene areas were formed by the temperature decreasing from 900 °C. These results show that we can observe the dissolution and regrowth of graphene by using OM in-situ observation.

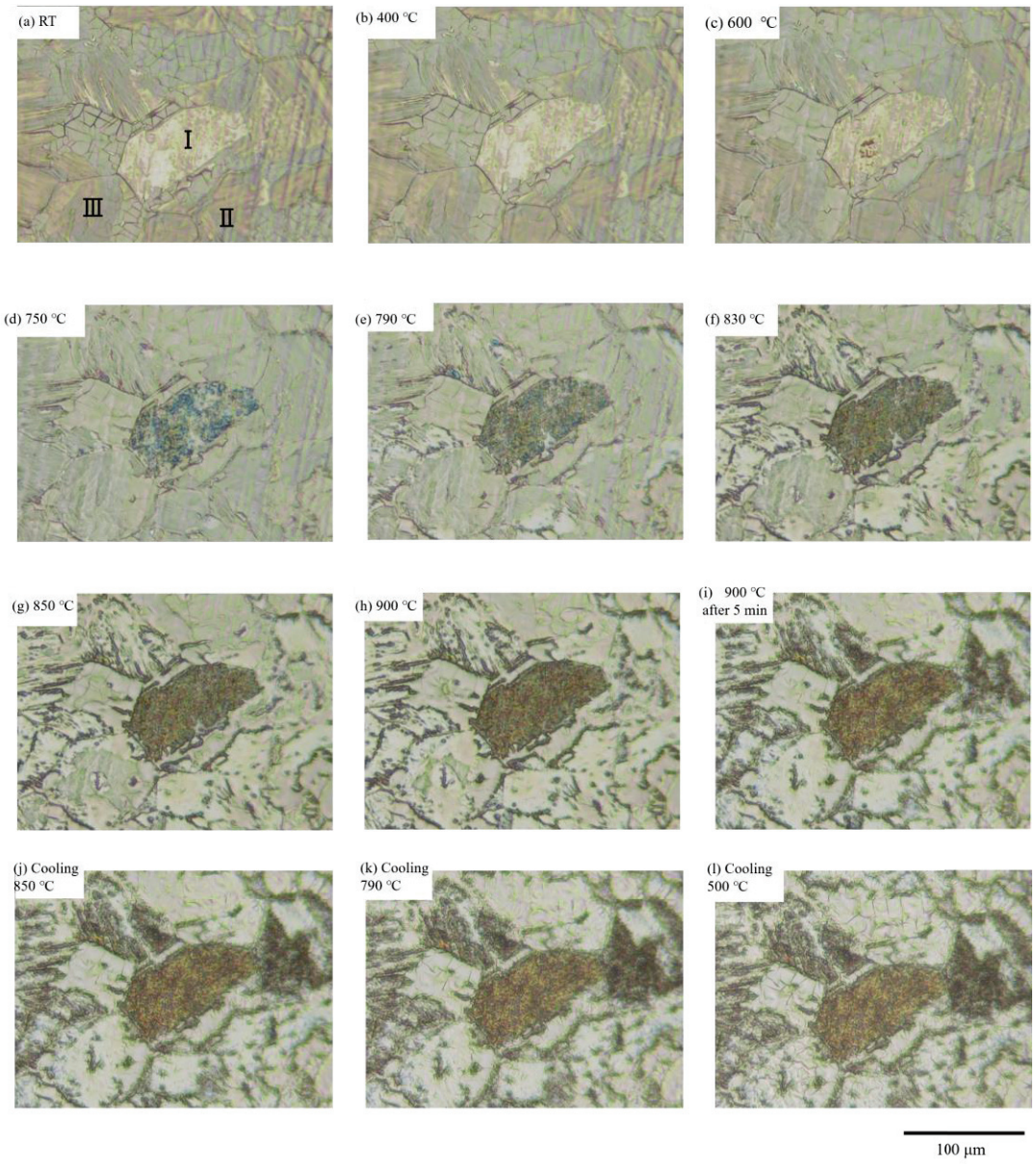

Fig. 28 In-situ OM images of CVD-grown graphene on the Ni sample surface during temperature rising and decreasing in vacuum.

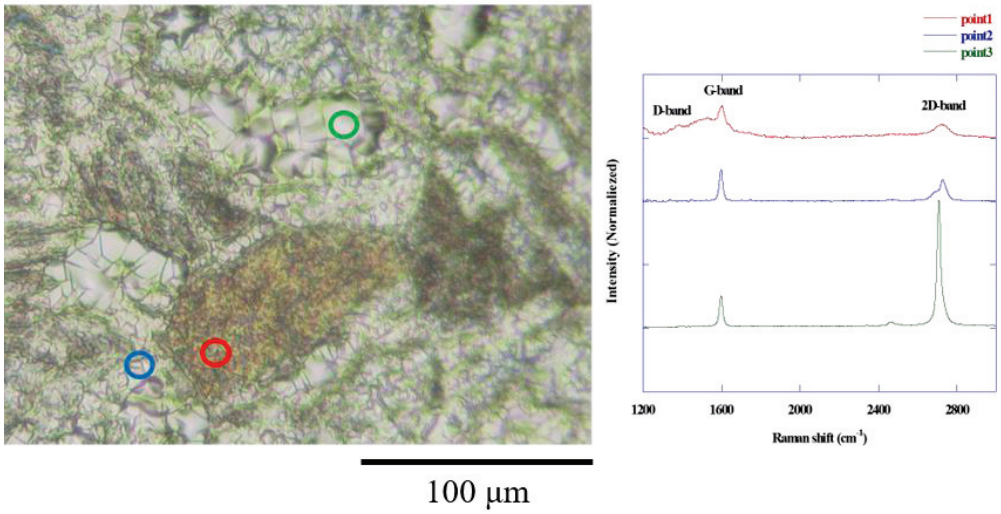

(a) (b)

Fig. 29 The sample after heating in vacuum and cooling to RT

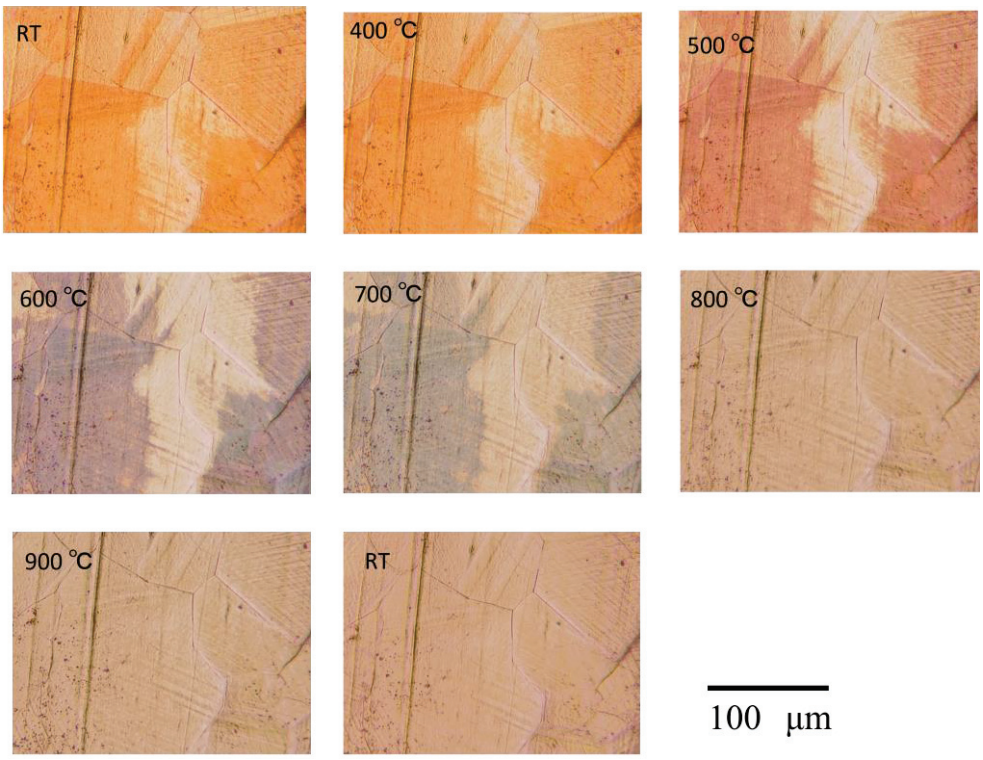

Fig.30 In-situ OM images of CVD-grown graphene on the Cu sample surface during temperature rising in vacuum.

In-situ observation of graphene on copper (Cu) was shown in Fig. 30, which with almost single layer graphene. Similar to the Ni sample, the surface showed no particular change up to 400 °C. The color changed as the temperature exceeded 500 °C, due to the gas escaping from the interface between graphene and the Cu substrate. While heating to 800 °C, the surface began keeping as the same. Graphene is stable till 900 °C on Cu substrate, and no dissolution occurred as on Ni substrate. This results is also an evidence of graphene stability at high temperatures [49,50] The results of Raman spectroscopy before and after heating of this sample are presented in the Fig. 31. The peak shift after heating may be due to metal distortion. Our results showed that Ni is not a suitable substrate for graphene growth and for heat treatment.

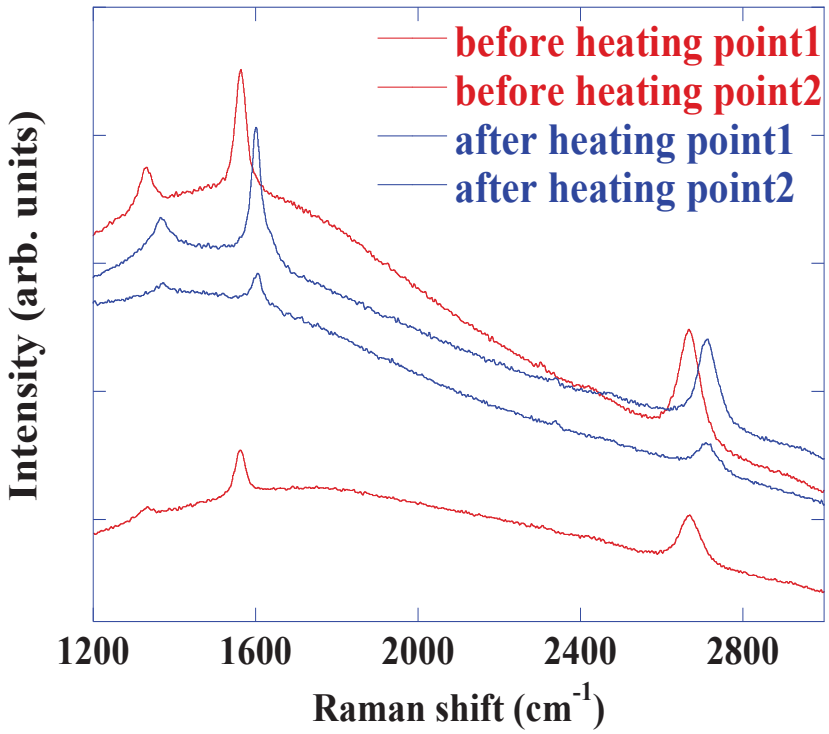

Fig.31 Raman spectra of CVD-grown graphene on the Cu sample.

3.5 In-situ observation in gas flow condition

Experiment with the same optical microscope observation system were conducted to see whether the state of etching can be observed in situ. The observation was performed with Ar + H_2 (5 %) gas (30 ml/min) flowing. A sample of multilayer graphene deposited on Ni foil was prepared by ethanol chemical vapor deposition (CVD).

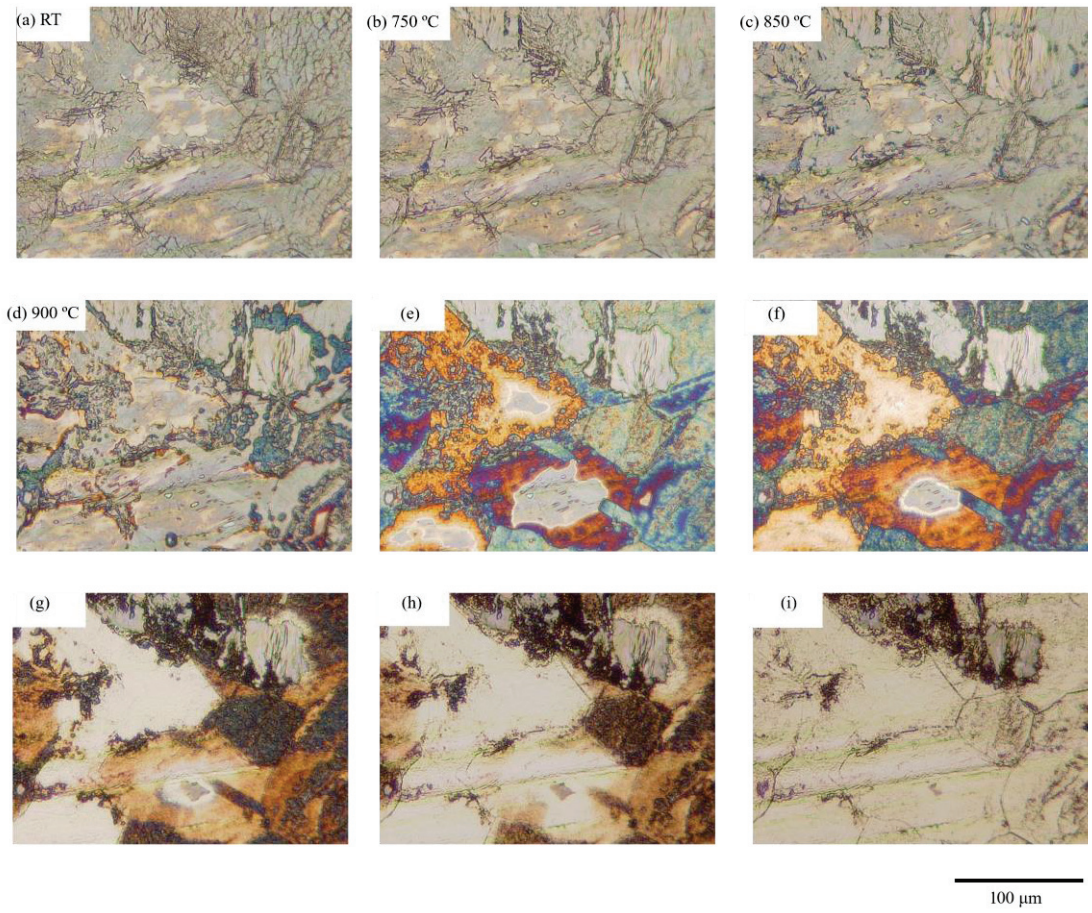

Fig.32 In-situ OM images of CVD-grown graphene on the Ni sample surface during temperature rising in Ar + H_2 atmosphere.

When the sample was heated in Ar + H_2, the dark blue and orange areas appeared on the sample surface. These areas are amorphous carbon (a-C) as shown in Fig. 32 (a) to (d). Half of graphene area was etched by the Ar + H_2 gas during the heating. While keeping the sample at 900 °C in

the atmosphere, the graphene was etched away gradually (Fig. 32 e~i). This reacting process was different from that in vacuum condition. When we used Ar gas only as shown in Fig.33, the in-situ observation was also different. The area of a-C on the sample surface could not be etched. It was seemed that the state of etching also depended on the crystal orientation of Ni. For example, as show in Fig. 32 (g), Ni had been partially etched, but there was still areas covered by graphene. One possible explanation is that the orientation of Ni domain was different.

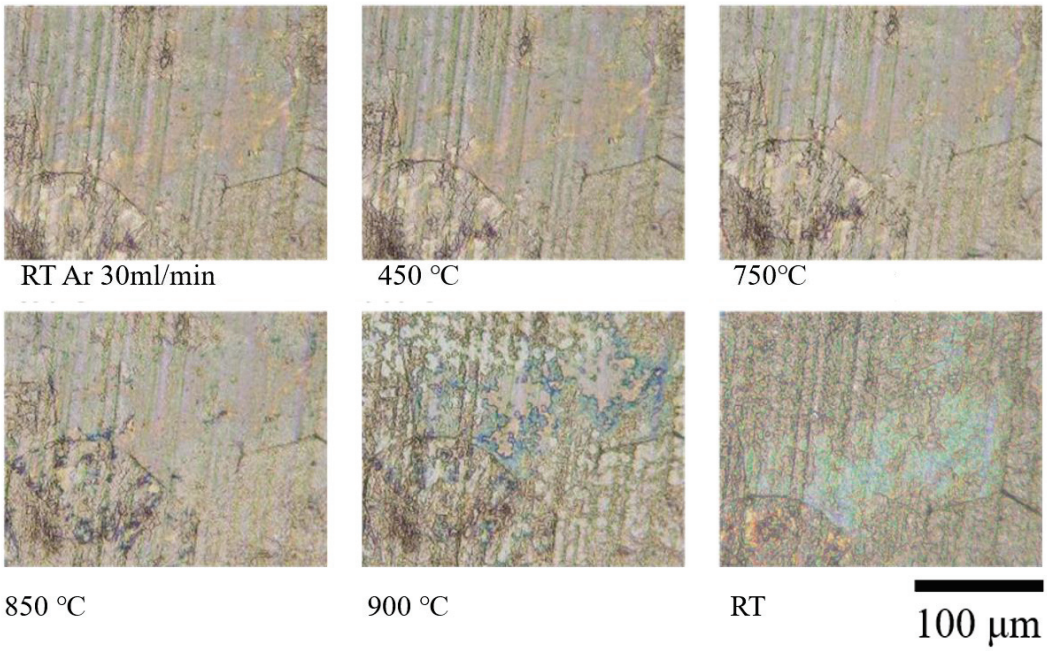

Fig. 33. In-situ OM images of CVD-grown graphene on the Ni sample surface during temperature rising in Ar atmosphere.

Summary

In chapter 3, in-situ observation of carbon growth by OM using a heating vacuum chamber was described. Graphene growth on a Ni domain could be recognized from the color change of the Ni surface in the optical image. A flat Ni surface and crystal orientation of the metal are important factors that allow growth of a large area graphene. In situ observation by OM is a simple and effective way of studying graphene growth. It will be used to understand the growth mechanism of graphene on various substrates. In addition, OM and Raman spectroscopy could be performed to observe the growth of graphene on the metal with atmospheric control in real time. Results derived from real-time observation of the color image provide a simple way of understanding the graphene state under various atmospheres.

Chapter 4. AFM induced local oxidation

4.1 About AFM anodic oxidation of graphene

Scanning probe microscopy (SPM) is a general term for microscope using a probe. It includes scanning tunneling microscopy (STM), atomic force microscopy (AFM), and magnetic force microscopy (MFM). In this chapter, experiments were carried out using an AFM. In AFM anode oxidation, water in air is cross-linked by applied an electric field on a probe of AFM and a sample surface, and conductivity occurs. When the voltage beyond a threshold is applied in here, the water was electrolyzed, and an ion reacts with the sample surface atoms. In the case of Si substrate, SiO_2 will be generated. This is a principle of AFM anode oxidation. We can control the applied bias voltage and the humidity of the sample chamber to control the pattern and size of the anodic oxidation areas. As the reaction is essentially an electrolysis, it may be foresaw of processing condition using an electrochemical approach such as theoretical decomposition voltage and reaction rate theory. In previous works, there was a group experimenting with AFM anodization, but presenting the case of oxidation, (generating GO) or etching as (getting CO_2). In this work, we showed that these two oxidation processes can be controlled voltage changing [51-55]. An anodic oxidation model was also proposed.

4.2 Sample for anodic oxidation

The starting samples are graphene/SiO_2/Si substrates. The sample of graphene was formed by the CVD method. These samples are two types, named as multilayer (thickness: 50 nm, 80-100 layers) and fewlayer (thickness: 2 nm, 1-4 layers), respectively. We carried out AFM oxidation on these two kind of samples at room temperature in a humidity of 20 %. The scan speed of the AFM probe was 10 nm/s. When a bias voltage was applied on the AFM probe, the water in the air was electrolyzed and the graphene was oxidized, which caused the raised and/or dented AFM images on the sample surface.

Figure 34 (a) shows the AFM images for the case of few layer graphene as an example. When the applied voltage was lower than 3 V, no change was observed. At the bias voltage between 2 V to 10 V, the graphene surface was raised and the graphene oxide (GO) was generated, as shown in Fig. 34 (b). Because of the volume size of GO was larger than that of graphene, we observed a thickness increase of the graphene surface.

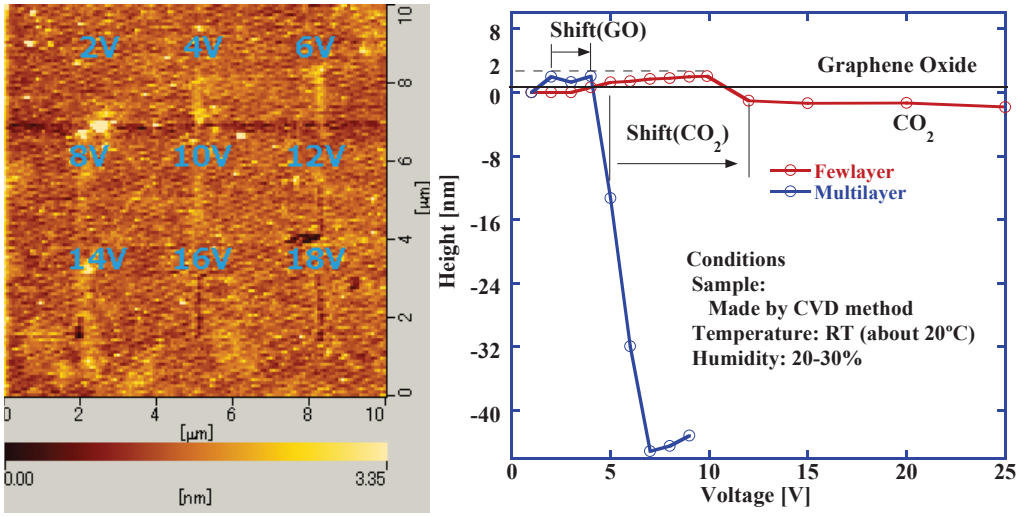

(a) (b)

Fig. 34 (a) AFM image of the raising and depressing surface of few layer graphene and (b) voltage dependence of multilayer and a few layer graphene sample in anodic oxidation

While the applied voltage exceeds 12 V, the carbon dioxide (CO_2) was generated, which led to a ditch generation in the AFM image. The graphene layer thickness was only ~ 2 nm, so we could see a saturation of the depth at voltage higher than 12 V. The formation voltages for GO and CO_2 were different for the few layer and multilayer graphene films, which will be summarized below.

4.3 Case of multilayer graphene sample

Figure 35 shows the applied bias voltage dependence of the surface height of multilayer graphene. At the bias voltage, lower than 1 V, no surface change

was observed. GO was generated at 2 - 4 V, with the raised surface. At the

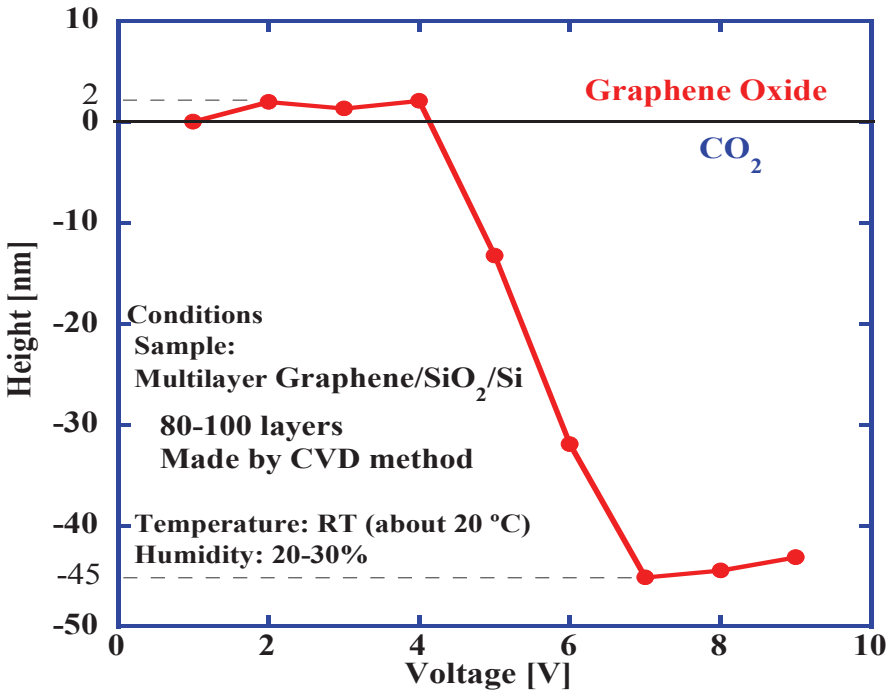

Fig. 35. Height with voltage of multilayer graphene

bias voltage higher than 5 V, CO_2 was generated and depressed surface occurred. The depth of opened holes increased with increasing voltage, and became constant at about 45 nm, which was the thickness of the graphene layer used here. Taking the electrolyzed voltage of water of 1.23 V into account, these results are in agreement with the proposed theory, which will be described later.

4.4 Case of few layer graphene sample

As described in Fig. 36, for fewlayer graphene, both the generation voltages of GO and CO_2 shifted to higher bias side. The bias voltage for the raising graphene surface was 4 V, and the depressing voltage was 12V, respectively. The GO generating voltage for fewlayer graphene was about 2 V higher than that of multilayer graphene. At the same time, the CO_2 generating voltage shifted from 5 V to 12 V. The hole depth of the fewlayer graphene saturated at 2 nm for bias voltage of 25 V, which was in good

agreement with the graphene layer thickness used in the experiments.

We can compare our results with that of Masubuchi et al. 51). In their paper, the raising voltage was 4 - 6 V, which was almost the same value as this work. Our saturation voltage of depression of fewlayer graphene was 25 V. A similar result was also reported by Giesbers et al. 53). Those results were used in the following calculation for the decomposition voltage (DV) of graphene by anodic oxidation.

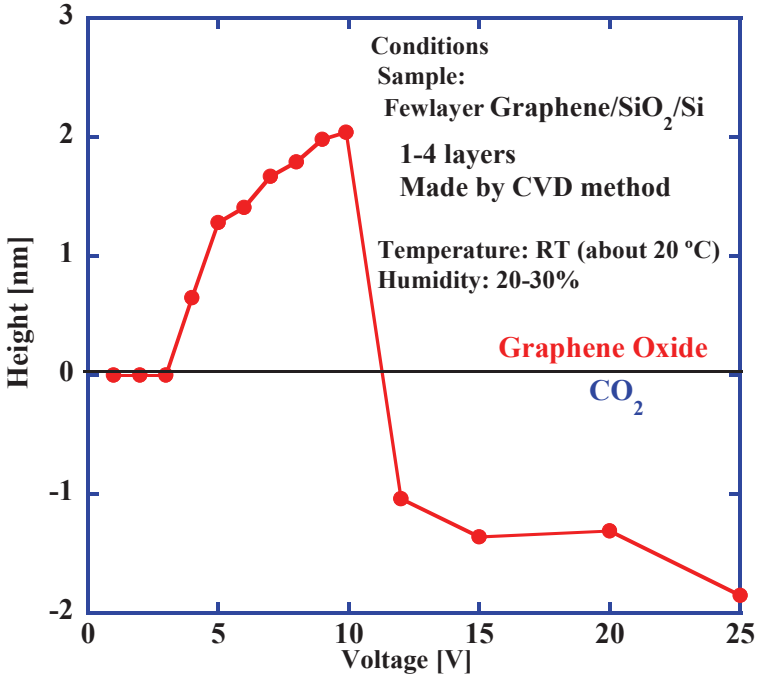

Fig. 36. Height with voltage of few layer graphene

4.5 Analysis and discussion

Referring to previous works [56-60], in general electrolysis reaction, the theoretical DV (TDV) is represented by equation 1.

$$TDV\ \ [V] = \frac{-\Delta G}{Fn} + \frac{RT}{Fn} \ln \frac{\alpha_X^x \alpha_Y^y}{\alpha_P^p \alpha_Q^q} \qquad (\ 1\ )$$

where ΔG is the Gibbs free energy, F is the Faraday constant, n is the amount of substance of electron for chemical reaction, R is the gas constant, T is the absolute temperature and α is the activity factor. We use this equation to calculate the DV for multilayer and fewlayer graphenes.

4.5.1 Case of Multilayer Graphene

In the case of multilayer graphene, the band structure is metallic and the layer is electrically conductive. Besides, reactants of H_2O and carbon from the graphene layers are sufficiently supplied. We can assume all the activities α_X, α_Y, α_P, α_Q as equal as one, then the second term of the equation becomes zero. Further, for the products of the oxidizing reaction of graphene, we consider the different case of CO_2 and GO.
Then, we calculated these two kinds of TDV for multilayer graphene. The structural change from graphene to GO is shown in Fig. 37.

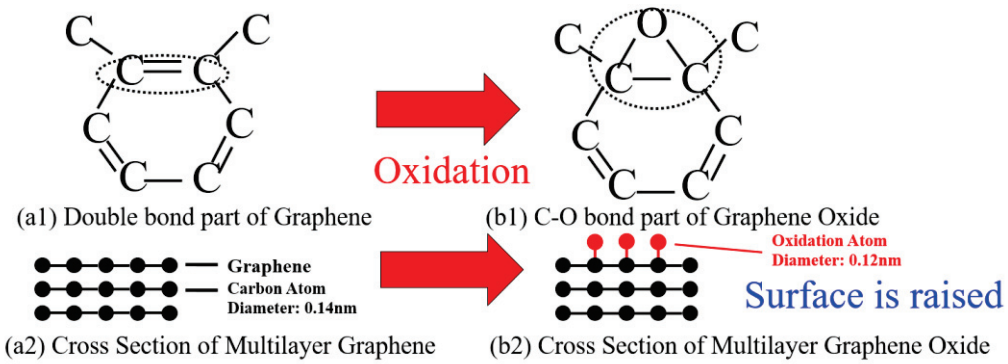

Fig 37. Structural change and reaction equations of graphene to graphene oxide

The generation of GO leads to the raise of graphene surface by bonding oxygen atoms to surface carbon atoms. The chemical and ionic equations of GO generation are shown in

$$(\mathrm{C}=\mathrm{C}+\mathrm{C}-\mathrm{C})/2+(\mathrm{H}-\mathrm{O}-\mathrm{H})\rightarrow(C-C+C-O\times2)+(H-H)$$

$$left\ \ side=(346+602)/2+459\times2=1392\ \ [\mathrm{kJ}/mol]$$

$$\text{right side } 346 + 358\times2 + 432 = 1494 \ [kJ/mol]$$

$$\Delta\text{H} = (\text{right side}) - (\text{left side}) = -102 \ [kJ/mol]$$

Entropy change is expressed in the next formula.

$$\Delta\text{S} = S_C^O + S_{H2O}^O - (S_{GO}^O + S_{H2}^O)$$

$$= 0.00574 + 0.00691 - (-0.09 + 0.1313) = 0.034 \ [kJ/mol \ K]$$

Therefore, the Gibbs' free energy in the normal temperature is

$$\Delta\text{G} = \Delta\text{H} - \text{T}\Delta\text{S} = -102 - 10 = -112 \ [kJ/mol]$$

Next, the number of moles of electrons that react on the anode and cathode is calculated:

$$(\text{Anode}): \ H_2O + 2C \rightarrow C_2O + 2H^+ + 2e^-$$
$$(\text{Cathode}): 2H_2O + 2e^- \rightarrow H_2 + 2OH^-$$

$$\text{TDV(GO)} = \frac{112\times10^3}{2\times96458} = 0.58 \ [V]$$

Therefore, the number of moles of the electron is 2. The chemical reaction is expected that GO is formed at theoretical decomposition voltage more than 0.58 volts. But it does not correspond to experimental value. Its gave energy $\Delta G^{\ddagger}$ bigger than ΔG for a reaction to advance actually, and had to be shifted to the mesomorphic state. Generation of oxidation graphene (GO) was considered as follows. First the OH^- which occurred by electrolyzing of H_2O combines in a C atom of graphene. After that H atom dissociates, and GO is generated. The activation energy is necessary by this process. We regarded the activation energy as that of the combination breaking energy of O-H, so we can take the activation energy as the binding energy of O-H, 459 kJ/mol. The electrode reaction is same as the one considered by theoretical decomposition voltage of aforementioned GO, so the number of moles of the electron will be 2. Therefore, when formula applied, the activation voltage shows to be the next,

$$\mathrm{ACV(GO)} = \frac{459\times10^3}{2\times96458} = 2.38\ \ [V]$$

GO was generated between 1 - 2 V in the actual experiment. The theoretical value is a little big, but is not biased so much. The case of CO_2 is equally calculated.

$$(\mathrm{C-O\times2 + C-C\times3}) + (\mathrm{H-O-H})$$
$$\rightarrow \big((\mathrm{C=C}) - (\mathrm{C-C})\big)\times4 + (\mathrm{C=O\times2}) + (\mathrm{H-H})$$

$$\text{left side} = 358\times2 + 346\times3 + 459\times2 = 2672\ \ [kJ/mol]$$

$$\text{right side} = (602-346)\times4 + 799\times2 + 432 = 3054\ \ [kJ/mol]$$

$$\Delta\mathrm{H} = (\text{left side}) - (\text{right side}) = -382\ \ [kJ/mol]$$

$$\Delta\mathrm{S} = S^O_{GO} + S^O_{H2O} - (S^O_C + S^O_{CO2} + S^O_{H2})$$
$$= -0.09 + 0.069 - (0.057 + 0.214 + 0.131) = 0.372\ \ [kJ/mol\ \ \mathrm{K}]$$

$$\Delta\mathrm{G} = \Delta\mathrm{H} - \mathrm{T}\Delta\mathrm{S} = -382 - 112 = -270\ \ [kJ/mol]$$

$$(\text{Anode}):\ H_2O + C_4O \rightarrow 3C + CO_2 + 2H^+ + 2e^-$$
$$(\text{Cathode}):\ 2H_2O + 2e^- \rightarrow H_2 + 2OH^-$$

$$\mathrm{TDV}\ \ (\mathrm{C}O_2) = \frac{270\times10^3}{2\times96458} = 1.40\ \ [V]$$

$$\mathrm{ACV}\ \ (\mathrm{C}O_2) = \frac{948\times10^3}{2\times96458} = 4.91\ \ [V]$$

By deriving the Gibbs energy, as shown in these equations, we get the theoretical DV of 0.270 V. In fact, GO is generated after the electrolyzing of water at 1.23 V, which gives rise to the raising voltage at about 2 V.

Figure 38 shows the structural change from graphene to CO_2. In this case, the graphene is oxidized and lifted off from the surface, as shown by the cross section structure. By the similar calculation as above, we can get the

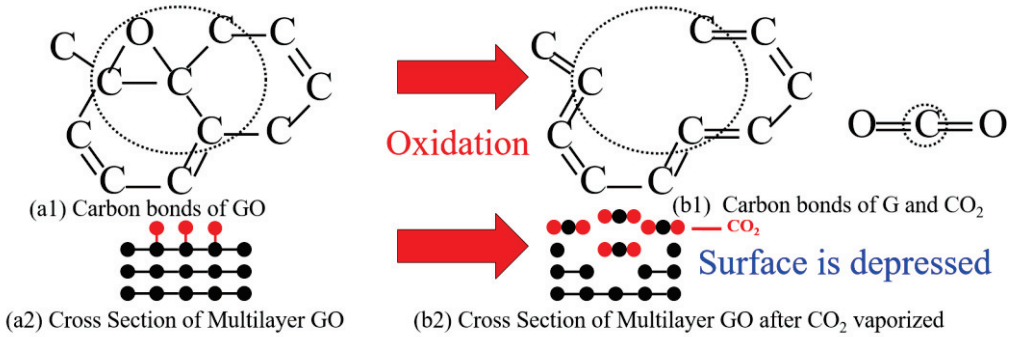

Fig. 38. Structural change and reaction equations of graphene to carbon dioxide

theoretical DV of 4.22 V, as shown in Fig. 34 by the starting depressing voltage of 5 V. In between DV of 2 V to 5V, the GO was generated and the graphene surface was raised.

4.5.2 Case of fewlayer graphene

In the experimental results of fewlayer graphene, reaction bias shifted to higher voltages. This is caused by the influence of the second term of Equation 1. Because the band structure of few layer graphene is semiconductive and the layer is hardly electrical conductive, the carbon atoms are also not efficiently supplied, we should assume the activities are dependent with the layer number.

Then, we calculated these two kinds of 2nd term of TDV for fewlayer graphene. In the case of GO generation, we do not know the true value of activity factor, so we assume activities as Equations 2.

$$\alpha_{H_2O} = 1(For\ \ solvent) \quad (\ 2.1\ )$$

$$\alpha_C = \alpha_X = \exp\left(\frac{-kN_{max}}{N} + 1\right) \quad (\ 2.2\ )$$

$$\alpha_{C_2O} = 1(For\ \ solid) \quad (\ 2.3\ )$$

$$\alpha_{H_2} = 1(For\ \ ion) \quad (\ 2.4\ )$$

Using those assumptions, the calculated result is presented by Equation 3.

$$2nd\ \ term\ \ of\ \ TDV_{GO} = \frac{RT}{nF}\ln\frac{\alpha_{C_2O}\alpha_{H_2}}{\alpha_C\alpha_{H_2O}}$$

$$= \frac{RT}{1\times F}\ln\left(\frac{1}{\alpha_X}\right)$$

$$= \frac{RT}{F}\left(\frac{kN_{max}}{N} - 1\right) \quad (\ 3\ )$$

From Equation 3, we can see that if layer number N is increased, the 2nd term will decrease. Similarly, in the case of CO_2 generation, we assume activities as Equations 4, the calculation is shown by Equation 5.

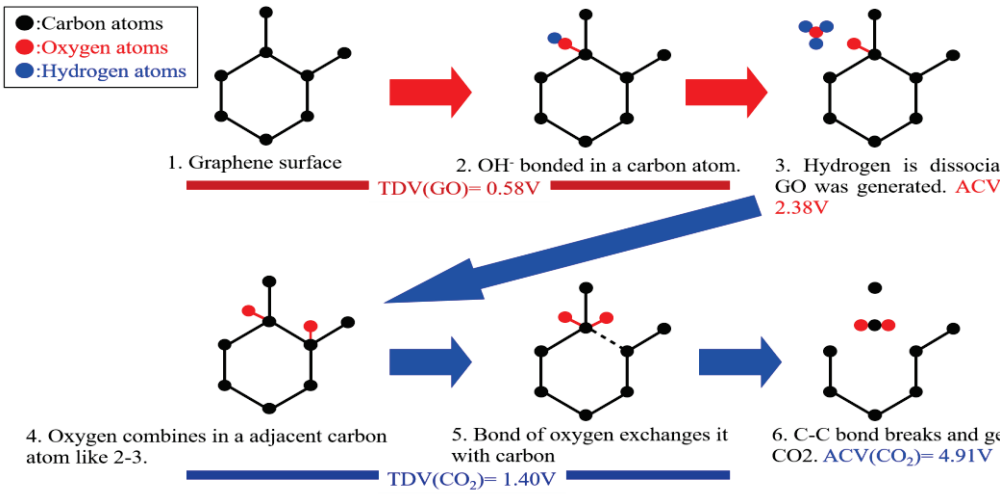

Fig. 39. Graphene Anodic oxidation model

$$\alpha_{H_2O} = 1 \ (For \ solvent) \quad (4.1)$$

$$\alpha_C = 1 \ (For \ solid) \quad (4.2)$$

$$\alpha_{C_4O} = \alpha_X^3 = \exp(3(\frac{-kN_{max}}{N} + 1))(For \ ion) \quad (4.3)$$

$$\alpha_{H_2} = 1 \ (For \ solid) \quad (4.4)$$

$$\alpha_{CO_2} = 1 \ (For \ gas) \quad (4.5)$$

$$2nd \ term \ of \ TDV_{CO_2} = \frac{RT}{nF} \ln \frac{\alpha_C^3 \alpha_{CO_2} \alpha_{H_2}}{\alpha_{C_4O} \alpha_{H_2O}^2}$$

$$= \frac{RT}{1 \times F} \ln(\frac{1}{\alpha_X^3})$$

$$= \frac{3RT}{F}\left(\frac{kN_{max}}{N} - 1\right) \quad (5)$$

A model for the anodic oxidation of graphene is shown in Fig. 39 from these calculation results. The calculations showed that the theoretical decomposition voltage of 0.58 V of GO corresponds to a reversible state, but an activation voltage of more than 2.38 V is needed for a continues oxidation. A voltage of more than 4.91 V (more than 1.40 V of the theoretical decomposition voltage) is necessary for the generation of CO_2 and for keeping the etching of multilayer graphene.

Table 2 shows the TDV against the value of kNmax. Nmax is the number of graphene layers for which the second term of equation 1 is negligible. From this, the TDVs for GO and CO_2 generation can be estimated. For example, when kNmax = 67, TDVs of GO and CO_2 for monolayer graphene (N = 1) are 4.09 V and 10.03 V, respectively. Also, TDV of bilayer graphene (N = 2) are 3.22 V and 7.43 V. The calculated results are almost

Table 2 Calculation of TDV with graphene layer number kN_{max}

	TDV[V](N=1)		N=2		N=80	
kN_{max}	GO	CO_2	GO	CO_2	GO	CO_2
67	4.09	10.03	3.22	7.43	2.38	4.91
92	4.73	11.97	3.54	8.40	2.38	4.92

$$TDV_{2nd_{GO}} = \frac{RT}{F}\left(\frac{kN_{max}}{N} - 1\right)$$

$$TDV_{2nd_{CO_2}} = \frac{3RT}{F}\left(\frac{kN_{max}}{N} - 1\right)$$

consistent with the experimental results. In contrast, a large layer number would lead to lower TDVs. When N = 80, as in the case of multilayer graphene used in this work, TDVs of GO and CO_2 are predicted to be 2.38 V and 4.91 V, respectively. From the results of calculated, Fig. 40 plots the TDV against the value of graphene layers. These are in good agreement with the experimental results.

Although the above-mentioned assumption of activities may need further refinement, the TDVs changed by the layer number are acceptable. Also the bonding manner of fewlayer graphene should be different from that of multilayer. But the discussion proposed here might give useful prediction when we carry out the nanoprocessing of graphene.

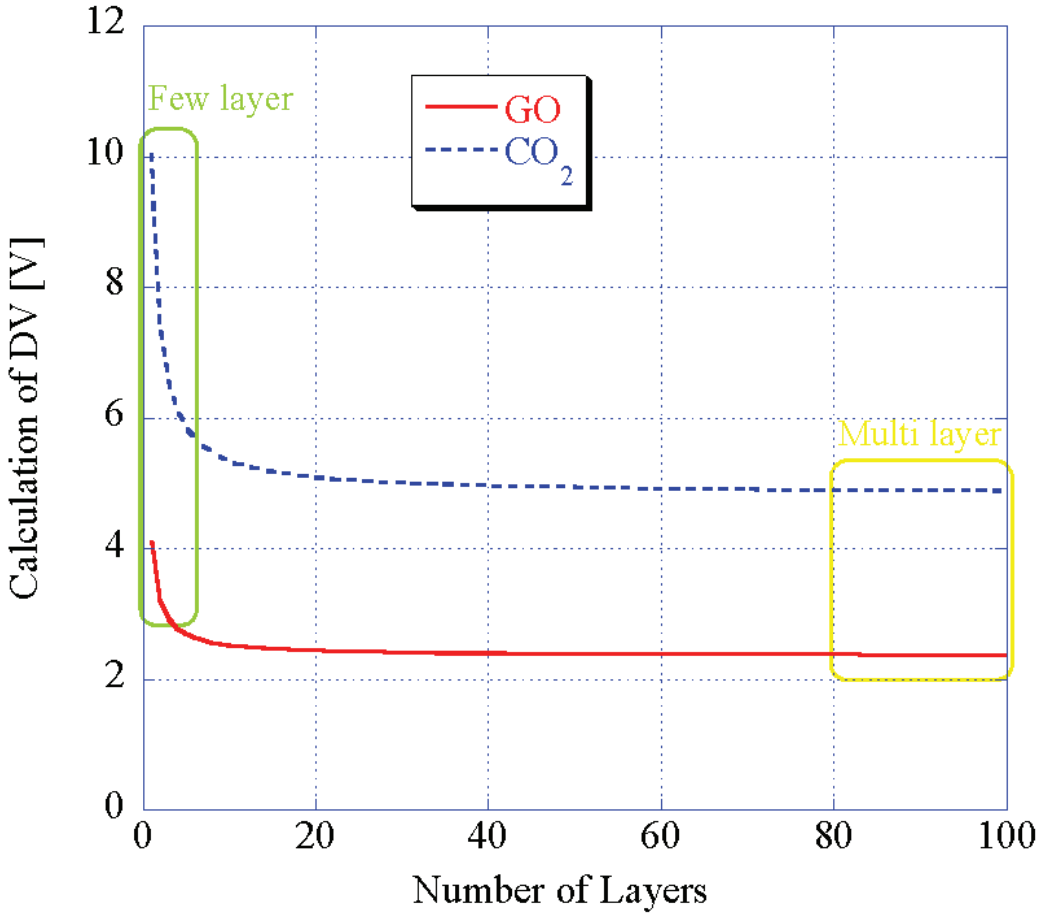

Fig. 40. Calculation of TDV with graphene layer number

Summary

In chapter 4, data on the rise and depression of few-layer and multilayer graphene samples were obtained by varying the applied voltage in the experiment of AFM anode oxidation. The calculated TDV roughly match the experimental results. Experimental results for multilayer graphene match the first term of the TDV equation. Values for few-layer graphene shifted to high voltages because of the second term and its band structure. Thus, conditions leading to raised or depressed surfaces changed with the thickness of graphene and the bias voltage. GO (rise) and CO_2 (depression) were produced by simultaneously changing the bias voltage at the same location. The oxidation model seems plausible, but two kinds of oxidation processes exist, named as, protuberance and collapse, which are strongly depending on the film thickness of graphene.

Raised parts of GO may be used in Schottky diode, while CO_2 from depressed regions may be used in etching and insulation. Therefore, a diode microcircuit on graphene can be constructed simply by anodic oxidation. As the reaction is oxidation, the process can be used not only by AFM, but also by various techniques such as nano-imprint lithography.

Chapter 5. Conclusion

In this paper, we investigated the growth and regrowth of graphene and carried out the in-situ observation of graphene growth by using an optical microscope (OM). We also performed the nanometer-sized oxidation of graphene by using an atomic force microscope (AFM). From these experiments, a simple way of understanding the growth and etching processes of graphene layers was proposed and demonstrated. The detail progress made by this study is summarized as follows.

Firstly, we proposed a new method of organic matter coating and annealing process to form graphene layers. Monolayer and multilayer graphene samples were fabricated on Ni substrates at relatively low temperatures. We chose the Orange II as the organic matter. It was decomposed at about 450 °C and remained carbon sources on the Ni surface. The remained carbon atoms were dissolved in Ni metal at about 900 °C, and extracted at the cooling procedure to form graphene. This temperature is about 200 °C lower than that of CVD growth. A model has been proposed and discussed.

Next, we proposed, for the first time, an in-situ observation of graphene growth by using the optical microscope (OM). The OM was equipped to a vacuum chamber with a heating stage. As the results, we first observed the dissolution and regrowth of graphene layers on the Ni surfaces only by using the visible light. Although the in-situ observation of graphene has been reported by using a scanning electron microscope (SEM), our method is simple and quick. The stability of graphene layers was also demonstrated by the same system. The graphene layers showed no dissolution on a Cu substrate and kept stable till 900 °C. But the graphene layer was easily etched in reactive atmosphere like H_2.

Finally, the anodic oxidation of graphene was carried out by using AFM induced oxidation. Different oxidizing manner for monolayer and multilayer graphene samples was demonstrated. The graphene makes oxide (GO) at low anodic oxidation voltages, but will be etched away by forming carbod dioxide (CO_2) at higher bias voltages. This technique can be used in nanoprocessing graphene layers to fabricate new devices.

As mentioned above, we have investigated the growth, regrowth,

oxidation and stability of graphne material. Although our results might be on the first steps, these should open a door for understanding this promising material and be useful for further devices applications. Further studies are highly expected.

Acknowledgment

This Ph.D. research was performed with the guidance and cooperation of many individuals. First, I thank the people who assisted with the laboratory equipment. I gained much experience and met many excellent people along the way. I would like to mention them here.

I would like to thank my supervisor, Professor Xinwei Zhao, of the Tokyo University of Science. I spent six years in his laboratory studying graphene and acquiring the skills of a researcher. Without his continuous support and communication, I could not have finished my work.

My special thanks are due to Professor Yoshikazu Homma and Assistant Professor Hiroki Kato of Tokyo University of Science for their guidance and advice.

I also wish to thank previous and current members of the Zhao Laboratory. In particular, I would like to thank my coworkers, Mr. Tatsuya Kobayashi, Mr. Kenichi Uki, Ms. Miku Nishimura, Mr. Akinobu Ono, Mr. Junpei Noguti, and Mr. Minoru Sakurai. I also would like to express my gratitude to previous and current graduate students who worked at the lab, namely, Mr. Keiichi Ikegami, Mr. Toshiki Ohkane, Mr. Keita Ooka, Mr. Tsutomu Obata, Mr. Takuya Ohtsuki, and Dr. Susumu Harako. They have been great colleagues and some of them have sometimes been companions during long vacations in summer.

Finally, I would like to show my appreciation to everyone else who had helped me. Without their support, it would have been impossible for me to finish this work and completed my doctoral thesis.

References

1. Novoselov, K. S., Geim, A. K., Morozov, S. V., Jiang, D., Zhang, Y., Dubonos, S. V., Grigorieva, I.V., and Firsov, A. A.., science, **306**(5696), 666-669. (2004).

2. Wallace, Philip Richard., Physical Review **71**.9, 622, (1947).

3. Slonczewski, J. C., and P. R. Weiss., Physical Review **109**.2, 272. (1958)

4. Hernández-Ortíz, S., G. Murguía, and A. Raya., Journal of Physics: Condensed Matter **24**.1: 015304. (2011)

5. Novoselov, K. S. A., Geim, A. K., Morozov, S., Jiang, D., Katsnelson, M. I, Grigorieva, I. V., Dubonos, S. V. and Firsov, A. A., nature, **438**(7065), 197-200, (2005).

6. Zhang, Y., Tan, Y. W., Stormer, H. L., & Kim, P., Nature, **438**(7065), 201-204. (2005).

7. Kim, K. S., Walter, A. L., Moreschini, L., Seyller, T., Horn, K., Rotenberg, E., & Bostwick, A. Nature materials, **12**(10), 887-892. (2013).

8. Nair, R. R., Blake P., Grigorenko, A. N., Novoselov, K. S., Booth, T. J., Stauber, T., Peres, N. M. R. and Geim, A. K. Sience **320**, 1308 (2008).

9. C. Casiraghi, A. Hartschuh , E. Lidorikis , H. Qian , H. Harutyunyan , T. Gokus , K. S. Novoselov and A. C. Ferrari.Nano Lett. **7**, 2711–2717 (2007).

10. Zhipei Sun, Tawfique Hasan, Felice Torrisi, Daniel Popa, Giulia Privitera, Fengqiu Wang, Francesco Bonaccorso, Denis M. Basko and Andrea C. Ferrari. ACS Nano **4**,803–810 (2010).

11. P. Blake, E. W. Hill, A. H. Castro Neto, K. S. Novoselov, D. Jiang, R. Yang, T. J. Booth and A. K. Geim. Appl. Phys. Lett. **91**, 063124 (2007).

12. Yoon, H. J., Yang, J. H., Zhou, Z., Yang, S. S., & Cheng, M. M. C. Sensors and Actuators B: Chemical, **157**(1), 310-313. (2011)

13. El-Kady, M. F., Strong, V., Dubin, S., & Kaner, R. B. Science, **335**(6074), 1326-1330. (2012).

14. Li, X., Zhu, H., Wang, K., Cao, A., Wei, J., Li, C., Jia,Y., Li, Z., Li, X., & Wu, D. Advanced Materials, **22**(25), 2743-2748. (2010).

15. Heejun Yang, Jinseong Heo, Seongjun Park, Hyun Jae Song, David H. Seo, Kyung-Eun Byun, Philip Kim, Science **336**, 1140 (2012)

16. Keun Soo Kim, Yue Zhao, Houk Jang, Sang Yoon Lee, Jong Min Kim, Kwang S. Kim, Jong-Hyun Ahn, Philip Kim, Jae-Young Choi & Byung Hee Hong, Nature **457**, 706-710 (2009)

17. T. S. Sreeprasad, Alfredo Alexander Rodriguez, Jonathan Colston, Augustus Graham, Evgeniy Shishkin, Vasanta Pallem, and Manhattan, Kansas, Nano Lett. **13**(4), 1757-1763, (2013)

18. Huc, V., Bendiab, N., Rosman, N., Ebbesen, T., Delacour, C., & Bouchiat, V. Nanotechnology, **19**(45), 455601. (2008)

19. E. G. Acheson, Manufacture of Graphite, U.S. Patent 615648, (1896).

20. A. J. Van Bommel, J. E. Crombeen and A. Van Tooren, Surf. Sci., **48**, 463–472. (1975).

21. W. A. de Heer, C. Berger, M. Ruan, M. Sprinkle, X. Li,Y. Hu, B. Zhang, J. Hankinson and E. Conrad, Proc. Natl. Acad. Sci. U. S. A., **108**, 16900–16905. (2011).

22. Bae, S., Kim, H., Lee, Y., Xu, X., Park, J. S., Zheng, Y., Balakrishnam, J., Lei, T,. Kim, R. H., Song, I. Y., Kim, J. Y., Kim, S. K., Özyilmaz, B., Ahn, J. H., Hong, H. B., & Iijima, S. Nature nanotechnology, **5**(8), 574-578. (2010).

23. Baraton, L., He, Z. B., Lee, C. S., Cojocaru, C. S., Châtelet, M., Maurice, J. L., Lee, H. Y., & Pribat, D. EPL (Europhysics Letters), **96**(4), 46003. (2011).

24. Wang, Y., Page, A. J., Nishimoto, Y., Qian, H. J., Morokuma, K., & Irle, S. Journal of the American Chemical Society, **133**(46), 18837-18842. (2011).

25. Mattevi, C., Kim, H., & Chhowalla, M. Journal of Materials Chemistry, **21**(10), 3324-3334. (2011).

26. Li, X., Magnuson, C. W., Venugopal, A., An, J., Suk, J. W., Han, B., Borysiak, M., Cai, W., Velamalanni, A., Zhu, Y,. Fu, L., Vogel, M. E., Voelkl, E., Colombo, L., & Ruoff, R. S. Nano letters, **10**(11), 4328-4334. (2010).

27. Mohammad Choucair, Pall Thordarson & John A. Stride. Nature Nanotechnology **4**, 30 - 33 (2009).

28. Valeria Alzari,Daniele, Nuvoli,Sergio, Scognamillo, Massimo Piccinini, Emilia Gioffredi,Giulio Malucelli, Salvatore Marceddu,Mario Sechi, Vanna Sanna and Alberto Mariani.J. Mater. Chem. **21**, 8727-8733. (2011).

29. Liying Jiao, Li Zhang, Xinran Wang, Georgi Diankov & Hongjie Dai.Nature **458**, 877-880. (2009).

30. Dmitry V. Kosynkin, Amanda L. Higginbotham, Alexander Sinitskii, Jay R. Lomeda, Ayrat Dimiev, B. Katherine Price & James M. Tour.Nature **458**, 872-876 (2009).

31. Zhang, Y., Gomez, L., Ishikawa, F. N., Madaria, A., Ryu, K., Wang, C., ... & Zhou, C. The Journal of Physical Chemistry Letters, **1**(20), 3101-3107. (2010).

32. Safron, N. S., & Arnold, M. S. Journal of Materials Chemistry C, **2**(4), 744-755. (2014).

33. Satoru Suzuki, Yusuke Takei, Kazuaki Furukawa, and Hiroki Hibino. Applied Physics Express **4**. 6. 065102. (2011).

34. Nakazawa, Hideki, and Maki Suemitsu. Journal of applied physics **93**.9 5282-5286. (2003).

35. Suemitsu, M., and H. Fukidome. Journal of Physics D: Applied Physics **43**.37. 374012. (2010)

36. Lemme, M. C., Bell, D. C., Williams, J. R., Stern, L. A., Baugher, B. W., Jarillo-Herrero, P., & Marcus, C. M. ACS nano, **3**(9), 2674-2676. (2009).

37. Boden, S. A., Moktadir, Z., Bagnall, D. M., Mizuta, H., & Rutt, H. N. Microelectronic Engineering, **88**(8), 2452-2455. (2011).

38. Leonardo C. Campos, Vitor R. Manfrinato, Javier D. Sanchez-Yamagishi, Jing Kong, and Pablo Jarillo-Herrero. Nano Lett., vol. **9**, pp.2600-2604, (2009).

39. D. C Bell, M C Lemme, L A Stern, J RWilliams and C M Marcus. Nanotechnology, vol.**20**, 455301, (2009).

40. D.F. Michael, D. Marija, Appl. Phys. Lett., vol.**93**. 113107, (2008).

41. Andrea C. Ferrari & Denis M. Basko, Nature Nanotechnology, **8**, 235-246, (2013).

42. D. Graf, F. Molitor, K. Ensslin, C. Stampfer, A. Jungen, C. Hierold, and

L. Wietz, Nano Lett., **7**, 238-242. (2007).

43. Lewis, I. C. Carbon **20**.6: 519-529. (1982).

44. K.F. Lang, H. Buffleb, J. Kalowy. Chem. Ber., **90,** p. 2888, (1957)

45. Takahashi, K., Yamada, K., Kato, H., Hibino, H., & Homma, Y. Surface Science, **606** (7), 728-732. (2012).

46. Nakahara, H., Fujita, S., Minato, T., Saito, Y. e-Journal of Surface Science and Nanotechnology Vol. **14**. 39-42. (2016)

47. Zhenhua Ni, Yingying Wang, Ting Yu, and Zexiang Shen, Nano Res, 1, 273 291,(2008).

48. P. Blake, E. W. Hill, A. H. Castro Neto, K. S. Novoselov, D. Jiang, R. Yang, T. J. Booth, and A. K. Geim, APL, **91**, 063124, (2007)

49. Da Hee Jung, Cheong Kang,Minjung Kim,Hyeonsik Cheong,Hangil Lee,and Jin Seok Lee,J. Phys. Chem. C, **118**, 3574−3580. (2014).

50. L. Baraton, Z. B. He, C. S. Lee, C. S. Cojocaru, M. Chˆatelet, J.-L. Maurice1,Y. H. Lee and D. Pribat. EPL, **96**, 46003, (2011).

51. S. Masubuchi, Miho Arai and Tomoki Machida, Nano Lett, **11**, 4542-4546 (2011).

52. Lishan Weng. et al. Appl. Phys. Lett. **93**, 093107 (2008).

53. A.J.M. Giesbers, U. Zeitler, S. Neubeck, F. Freitag, K.S. Novoselov, J.C. Maan, Solid State Communications **147** 366-369 (2008).

54. Soeren Neubeck, Frank Freitag, Rui Yang, and Kostya S. Novoselov, Phys. Status Solidi B **247**, Nos. 11-12, 2904-2908 (2010).

55. Byun, I. S. et al.. ACS Nano **5,** 6417–6424 (2011).

56. J. A. Dagata, F. Perez-Murano, G. Abadal, K. Morimoto, T. Inoue, J. Itoh, and H. Yokoyama, Appl. Phys. Lett. **76**, 2710-2712 (2000).

57. Charles A. Goss, Jay C. Brumfield, Eugene A. Irene, and Royce W. Murray, Anal. Chem. **65**, 1378-1389 (1993).

58. Bailin Zhang and Erkang Wang, Electrochimica Acta. Vol.**40**, No.16, pp.2621-2633, (1995).

59. M. Luna, J. Colchero, and A. M. Baro, J. Phys. Chem. B **103**, 9576-9581 (1999).

60. Hyun-Suk Choo, Taro Kinumoto, Soon-Ki Jeong, Yasutoshi Iriyama,Takeshi Abe, and Zempachi Ogumi, Journal of The Electrochemical Society, **154** 10 B1017-B1023 (2007).

Appendix A : List of publications

(papers)

1. "Fabrication of graphene and graphite thin films from organic coating."
Mikihiro Kato, Kenichi Uki, Susumu Harako, Xinwei Zhao
Microelectronic Engineering 121 (2014): 96-99.

2. "A prospect for applications of graphene fabricated from an organic solution."
Mikihiro Kato, Miku Nishimura, Kenichi Uki, Susumu Harako, Xinwei Zhao
Microelectronic Engineering 141 (2015): 280-284.

3. "AFM Induced Local Oxidation of HOPG."
K. Uki, M. Kato, S. Harako, X. Zhao
MRS Proceedings. Vol. 1586. Cambridge University Press, 2014.

(International conference)

1. "A prospect for applications of graphene fabricated from an organic solution" Mikihiro Kato, Miku Nishimura, Kenichi Uki, Susumu Harako, and Xinwei Zhao. 40th International Conference on Micro and Nano Engineering, P-Fab-22, Lausanne, Switzerland, September 2014.

2. "AFM Local Anodic Oxidation and Theoretical Decomposition Voltages of Few/Multi Layer Graphene", K. Uki, M. Kato, M. Nishimura, and X Zhao. 27th International Microprocesses and Nanotechnology Conference, 6P-7-23, Fukuoka, Japan. November, 2014

3. "In-situ observation of graphene growth by an optical microscope" Mikihiro Kato, Junro Takahashi, Hiroki Kato, Yoshikazu Homma, Akira Suzuki, Xinwei Zhao. 41st International Conference on Micro and Nano Engineering, Tue-A-p73, Hague, Netherlands, September 22, 2015.

4. ” Influence of the atmosphere on in-situ observation of heated graphene layers” M.Kato, K. Shihommatsu, Y.Homma and X.Zhao. The 18th International Conference on Crystal Growth and Epitaxy, Fr1-G09-3, Nagoya Japan August 7th -12th ,2016

5. ” The in-situ observation graphene with gas flowing” Mikihiro Kato, Junro Takahashi, Yoshikazu Homma and Xinwei Zhao. 42th International Conference on Micro and Nano Engineering, Wen -B6-120, Vienna, Austria, 19-23 September 2016

(Domestic conference)

1. 「塗布を用いたグラフェンの作製 II」加藤幹大, 宇木権一, 趙新為、秋期第 74 回応用物理学会学術講演会、16p-P7-22、同志社大学（京都府）、9 月、2013 年

2. 「塗布を用いたグラフェンの作製 III」加藤幹大, 西村未来, 宇木権一, 趙新為、第 61 回応用物理学会春季学術講演会 17a-E2-3、青山学院大学（神奈川県）、3 月、2014 年

3. 「塗布を用いた絶縁基板上への直接成長グラファイト薄膜」加藤幹大, 西村未来、宇木権一, 趙新為、秋期第 75 回応用物理学会秋季学術講演会、19a-B3-2、北海道大学（札幌）、9 月、2014 年

4. 「塗布を用いた絶縁基板上への直接成長グラファイト薄膜 II」加藤幹大, 西村未来、趙新為、春期第 62 回応用物理学会春季学術講演会、11a-P6-5、東海大学（神奈川県）、3 月、2015 年

5. 「有機物塗布によるグラフェンの成長その場光学観察」加藤幹大, 西村未来、加藤大樹, 趙新為、秋期第 76 回応用物理学会秋季学術講演会、16a-PA2-31、名古屋国際会議場（愛知県）、9 月、2015 年

6. 「金属上の多層グラフェンのその場光学観察」加藤幹大, 高橋惇郎、本間芳

和、趙新為、春期第 63 回応用物理学会春季学術講演会、20p-S011-16、東京工業大学（東京都）、3 月、2016 年

7. 「多結晶ニッケル上の多層グラフェンのその場光学顕微鏡観察」加藤 幹大、四本松　康太、本間　芳和、趙　新為、秋期第 76 回応用物理学会秋季学術講演会、13p-P5-22、朱鷺メッセ（新潟県）、9 月、2016 年